

4. Celestial Mechanics

4.1 Kepler's Laws

Given a two-body problem--the Earth around the Sun, or a satellite around the Earth, with other factors neglected--one can easily show that the satellite moves around the source of attraction (or more accurately, around the center of mass of the two bodies) in an **ellipse**, with the center at one focus. That is Kepler's **first law**, published in 1609 and based on naked-eye observations of Mars by Tycho de Brahe. The **second law** ("law of areas") describes the way the motion of a satellite or a planet accelerates as it approaches the center of attraction: the "radius vector" connecting it to the center sweeps equal areas in equal times. The **third law** (1619) states that the square of the orbital period is proportional to the cube of the mean distance.

The laws themselves are derived relatively easily (below), but the full solution of the orbital motion is a bit more involved.

4.1.1 The first and second law

Let m_1 be the mass of the Earth and m_2 of the satellite (or of Sun and Earth, respectively), and let $(\mathbf{r}_1, \mathbf{r}_2)$ be their positions in some arbitrary system of coordinates. The attraction between the two will be along the vector $\mathbf{r} = \mathbf{r}_2 - \mathbf{r}_1$ from the center of the Earth to the satellite, always directed towards the other body. From Newton's law

$$\begin{aligned} m_1 \frac{d^2 \mathbf{r}_1}{dt^2} + \frac{G m_1 m_2}{r^3} (\mathbf{r}_2 - \mathbf{r}_1) &= 0 \\ m_2 \frac{d^2 \mathbf{r}_2}{dt^2} + \frac{G m_1 m_2}{r^3} (\mathbf{r}_1 - \mathbf{r}_2) &= 0 \end{aligned} \quad (8)$$

where G is the constant of gravitation. Cancel m_1 in the first equation, m_2 in the second, and subtract. If we then define

$$\mu = G(m_1 + m_2) \approx G m_1$$

then

$$\frac{d^2 \mathbf{r}}{dt^2} + \frac{\mu}{r^3} \mathbf{r} = 0 \quad (9)$$

The cross-product with \mathbf{r} gives the conservation of angular momentum

$$\frac{d^2 \mathbf{r}}{dt^2} \times \mathbf{r} = 0 = \left(\frac{d^2 \mathbf{r}}{dt^2} \times \mathbf{r} \right) + \left(\frac{d\mathbf{r}}{dt} \times \frac{d\mathbf{r}}{dt} \right) = \frac{d}{dt} \left(\frac{d\mathbf{r}}{dt} \times \mathbf{r} \right) \quad (10)$$

hence

$$\mathbf{h} = \mathbf{r} \times \frac{d\mathbf{r}}{dt} = \text{const.} \quad (11)$$

This is really the law of areas, since $h = |\mathbf{h}|$ is the area swept by the radius vector per unit time. The fact the vector \mathbf{h} is conserved shows that the motion stays in the same plane, normal to \mathbf{h} .

The value of μ is readily derived by noting that at the surface of the Earth, $r = R_E$, the acceleration due to gravity is g . Then

$$\frac{G m_1}{R_E^2} = g = \frac{\mu}{R_E^2} \quad (12)$$

Cross-multiply (2) by \mathbf{h}

$$\begin{aligned}\frac{d^2\mathbf{r}}{dt^2} \times \mathbf{h} &= -\frac{\mu}{r^3} (\mathbf{r} \times \mathbf{h}) = -\frac{\mu}{r^3} \mathbf{r} \times \left(\mathbf{r} \times \frac{d\mathbf{r}}{dt} \right) = \\ &= -\frac{\mu}{r^3} \left[\mathbf{r} \left(\mathbf{r} \cdot \frac{d\mathbf{r}}{dt} \right) - r^2 \frac{d\mathbf{r}}{dt} \right] = \mu \frac{d}{dt} \left(\frac{\mathbf{r}}{r} \right)\end{aligned}\quad (13)$$

Since $d\mathbf{h}/dt = 0$, the left-hand side of (13) is $d/dt [\mathbf{r} \times d\mathbf{r}/dt]$, allowing one to integrate (11) to

$$\frac{d\mathbf{r}}{dt} \times \mathbf{h} = \frac{\mu}{r} (\mathbf{r} + r\mathbf{e}) \quad (14a)$$

with \mathbf{e} a constant vector. Create the scalar product with \mathbf{r}

$$\mathbf{r} \cdot \left(\frac{d\mathbf{r}}{dt} \times \mathbf{h} \right) = \left(\mathbf{r} \times \frac{d\mathbf{r}}{dt} \right) \cdot \mathbf{h} = h^2 = \mu r + \mu r e \cos f \quad (14b)$$

with f the **angle** between \mathbf{e} and \mathbf{r} . From this the motion follows an ellipse

$$r = \frac{p}{1 + e \cos f} \quad (15)$$

with “parameter” (or *semi-latus rectum*) p

$$p = h^2/\mu \quad (16)$$

The angle f is called the **true anomaly** of the satellite. Since r is smallest when $f=0$, the angle f is the one between \mathbf{r} and the major axis of the ellipse, measured from **perigee**, the point of closest approach between the satellite and the Earth. Let (r_1, r_2) be the distances of (perigee, apogee), at which $\cos f = (-1, 1)$. Then

$$r_1 = \frac{p}{1 + e} \quad r_2 = \frac{p}{1 - e} \quad (17)$$

The semi-major axis a is half the sum of the distances to the two foci. Hence

$$a = \frac{r_1 + r_2}{2} = \frac{p}{2} \left(\frac{1}{1 + e} + \frac{1}{1 - e} \right) = \frac{p}{1 - e^2}$$

from which

$$p = a(1 - e^2) \quad (18)$$

4.1.2 Energy

The **conservation of energy** follows from multiplying (2) with $d\mathbf{r}/dt = \mathbf{v}$

$$\frac{d\mathbf{r}}{dt} \cdot \frac{d^2\mathbf{r}}{dt^2} = -\frac{\mu}{r^3} \left(\frac{d\mathbf{r}}{dt} \cdot \mathbf{r} \right)$$

or

$$\frac{1}{2} \frac{d}{dt} (v^2) = -\frac{\mu}{2r^3} \frac{d}{dt} (r^2) = -\frac{\mu}{r^2} \frac{dr}{dt} = -\frac{d}{dt} \frac{\mu}{r}$$

Hence

$$v^2 - \frac{2\mu}{r} = \text{const} = W \quad (19)$$

For any compact object of mass m moving in the gravitational field, $mW/2$ is the total energy. If that object can reach infinity with a finite velocity, its kinetic energy there obviously equals $mW/2$, which means W is positive. For a gravitationally bound object, however, W is negative.

4.1.3 Kepler's Third Law

The second law states that the areal velocity--the rate at which the radius vector sweeps area--is constant. For if \mathbf{v} is resolved into orthogonal components in polar coordinates r and θ ($\theta = f$)

$$\frac{d\mathbf{r}}{dt} = \mathbf{v} = \hat{\mathbf{r}} v_r + \hat{\boldsymbol{\theta}} v_\theta \quad (20)$$

then

$$\mathbf{h} = \mathbf{r} \times \mathbf{v} = \hat{\boldsymbol{\phi}} r v_\theta \quad (21)$$

and by simple geometry, $h/2 = r v_\theta/2$ is the areal velocity. In a full period T the total area A of the ellipse is swept, hence

$$\frac{1}{2} h T = A = \pi a b \quad (22)$$

where a is the semi-major axis and b the semi-minor one.

In the drawing, $b = AC$. Since the sum of distances of any point on the ellipse from the two foci (B, B') is $2a$, $AB = a$. By (18), with (15), the perigee distance is

$$BD = \frac{a(1 - e^2)}{1 + e} = a(1 - e)$$

and since $CD = a$, $CB = ae$. Then by Pythagoras

$$b = AC = a(1 - e^2)^{1/2} \quad (23)$$

By (16) and (18)

$$h^2 = a(1 - e^2) \mu \quad (24)$$

Squaring (22) and substituting

$$\frac{1}{4} a \mu (1 - e^2) T^2 = \pi^2 a^2 (1 - e^2)$$

giving finally

$$T^2 = (4\pi^2/\mu) a^3 \quad (25)$$

which is Kepler's 3rd law. Using (2), eq. (25) may be rewritten

$$T^2 = (4\pi^2 R_E / g) (a/R_E)^3 \quad (26)$$

Inserting the constants:

$$T_{\text{sec}} = 5063.48 (a/R_E)^{3/2} \quad (27)$$

4.2 Two-body motion in the orbital plane

As stated, the true anomaly f is the polar angle around the center of attraction, and by (15) and (18)

$$r = \frac{a(1 - e^2)}{1 + e \cos f} \quad (28)$$

The angle f does not vary uniformly, however. The way it varies is implicit in the law of areas

$$h = r^2 \frac{df}{dt} = \text{constant} \quad (29)$$

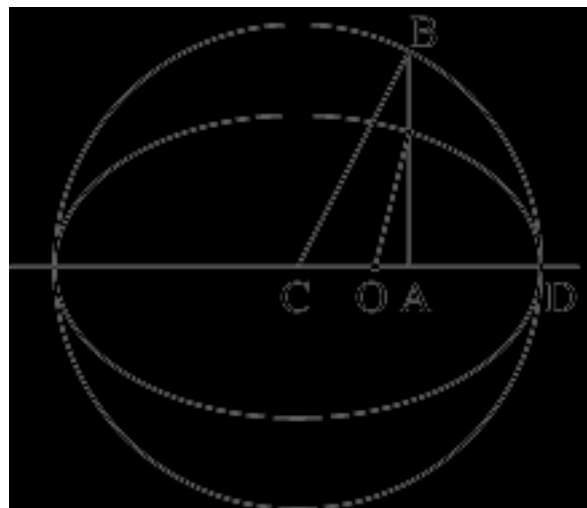
but isolating it from there is a bit involved.

The calculation below traces the connection between f and the **mean anomaly** l , an angle increasing like f by 2π each orbit but **linear** in time. The derivation of l traditionally uses an intermediate angle, the **eccentric anomaly** E which also grows by 2π each orbit. The relation between l and E involves a transcendental equation, named after Kepler, and that between E and f is not simple, either.

4.2.1 The Eccentric Anomaly

Unlike f , measured around the focus occupied by the center of attraction, the angle E is measured around the **center** C of the ellipse, the point halfway between the foci, and that is probably the reason for the name. Let a circle of radius a be drawn around C , enclosing the ellipse.

Then E is the angle between the major axis of the ellipse, also taken as the x -axis, and the radius to B , the projection of the satellite onto the circle, i.e. the point there having the same x as the satellite. Let:



O be the center of attraction

A the satellite's projection on the x -axis

P the satellite position

C the center of the circle (& ellipse) D the perigee point

Then $OP = r$ is the radius vector and

B its projection on the circle, with same x .

By (28)

$$AO = x = r \cos f \quad (30a)$$

$$e AO = er \cos f = a(1 - e^2) - r \quad (30b)$$

At perigee $\cos f = 1$ and by (28) the radius vector is

$$OD = a(1 - e) \quad (30c)$$

hence

$$OC = CD - OD = a - a(1 - e) = ae \quad (30d)$$

Also, because the radius of the circle centered at C is a

$$AC = a \cos E \quad (30e)$$

$$eAC = ea \cos E = e(CO + AO) = e^2a + a(1 - e^2) - r = a - r \quad (31)$$

giving

$$r = a(1 - e \cos E) \quad (32)$$

Equating this to

$$r = \frac{a(1 - e^2)}{1 + e \cos f} \quad (28)$$

allows $\cos E$ to be related to $\cos f$:

$$1 - e \cos E = (1 - e^2)/(1 + e \cos f) \quad (33)$$

$$\cos E = (e + \cos f)/(1 + e \cos f) \quad (34)$$

A more symmetric form is reached as follows. Eliminating the denominator in **(34)**

$$\cos E (1 + e \cos f) = e + \cos f \quad (35)$$

Add $(1 + e \cos f)$ to both sides

$$(1 + \cos E)(1 + e \cos f) = (e + \cos f) + (1 + e \cos f) = (1 + e)(1 + \cos f) \quad (36a)$$

Subtract $(1 + e \cos f)$

$$(1 - \cos E)(1 + e \cos f) = -(e + \cos f) + (1 + e \cos f) = (1 - e)(1 - \cos f) \quad (36b)$$

Divide:

$$\frac{1 - \cos E}{1 + \cos E} = \frac{1 - e}{1 + e} \frac{1 - \cos f}{1 + \cos f} \quad (37)$$

However, for any θ an identity exists

$$\tan \frac{\theta}{2} = \left[\frac{1 - \cos \theta}{1 + \cos \theta} \right]^{1/2} \quad (38)$$

hence

$$\tan \frac{E}{2} = \left[\frac{1 - e}{1 + e} \right]^{1/2} \tan \frac{f}{2} \quad (39)$$

For a result useful later, instead of dividing eqs. **(36)** by each other, multiply them:

$$\sin^2 E (1 + e \cos f)^2 = (1 - e^2) \sin^2 f \quad (40)$$

Then using **(28)**

$$\sin E = (r/a) (1 - e^2)^{-1/2} \sin f \quad (41)$$

4.2.2 The Mean Anomaly

The dependence of f on t is given by the law of areas, using **(16)**, **(18)** and **(21)**:

$$r^2 \frac{df}{dt} = h = \left[\mu a(1 - e^2) \right]^{1/2} \quad (42)$$

Now from **(39)**

$$\log \tan (E/2) = \log \tan (f/2) + \text{const} \quad (43)$$

and an identity exists (useful in integrating $1/\sin \theta$)

$$\frac{d}{d\theta} \log \tan \frac{\theta}{2} = \frac{1}{\sin \theta} \quad (44)$$

Thus the time derivative of **(43)** is

$$\frac{df}{dt} \frac{1}{\sin f} = \frac{dE}{dt} \frac{1}{\sin E} \quad (45)$$

With **(41)**

$$\frac{df}{dt} = \frac{dE}{dt} \frac{a}{r} [1 - e^2]^{1/2} \quad (46)$$

Multiplying by r^2 , applying **(42)** and canceling constants

$$r \frac{dE}{dt} = \left[\frac{\mu}{a} \right]^{1/2} \quad (47)$$

We may express r by

$$r = a(1 - e \cos E) \quad (32)$$

to get

$$\frac{d}{dt}(E - e \sin E) = \left[\frac{\mu}{a^3} \right]^{1/2} \quad (48)$$

A new constant may now be defined

$$n = \left[\frac{\mu}{a^3} \right]^{1/2} \quad (49)$$

and (48) can be integrated to

$$E - e \sin E = n(t - t_0) \quad (50)$$

This is *Kepler's equation*. As E grows from 0 to 2π , the lhs also grows from 0 to 2π , hence it will be identified with the *mean anomaly*

$$l = E - e \sin E \quad (51)$$

If T is the period

$$nT = 2\pi \quad (52)$$

and by (49)

$$T^2/a^3 = 4\pi^2/\mu = \text{const.} \quad (53)$$

This is Kepler's 3rd law, derived earlier from the law of areas.

4.3 The Position of a Satellite in its orbital Plane

4.3.1 Given the Orbital Elements

Suppose we know the orbital elements (a, e, l_0) at a time $t=0$, and need to find the position \mathbf{r} of the satellite and its velocity \mathbf{v} in the (ξ, η, ζ) frame. at some other time t . At that time, the mean anomaly is

$$l = l_0 + nt \quad (54)$$

and the eccentric anomaly satisfies

$$E - e \sin E = l \quad (51)$$

This can be solved numerically for E (see below). After that f could be obtained from

$$\tan \frac{E}{2} = \left[\frac{1-e}{1+e} \right]^{1/2} \tan \frac{f}{2} \quad (39)$$

but it may be simpler to use

$$r = a(1 - e \cos E) \quad (32)$$

to derive r . Then from (28)

$$\cos f = \frac{1}{e} \left[\frac{a(1-e^2)}{r} - 1 \right] \quad (55)$$

From this $\sin f$ is obtained, its sign depending on whether E is in the range $(0, \pi)$ or $(\pi, 2\pi)$, since f should be in that range too. Then

$$\xi = r \cos f \quad \eta = r \sin f \quad (56)$$

and of course $\zeta = 0$, since the satellite is always in its own orbital plane. Later, after the other orbital elements (i, ω, Ω) are introduced, it will also be possible to relate (ξ, η, ζ) to other coordinate systems, tied to the Earth and the Sun.

Kepler's equation is easily solved by **Newton's method**, a general iteration procedure. Suppose a solution is needed for a transcendental or high-order equation

$$f(x) = 0 \quad (57a)$$

and we know that x_0 is reasonably close to the solution. By Taylor expansion

$$f(x_0 + d) \approx f(x_0) + d \frac{df(x_0)}{dx} \quad (57b)$$

Suppose $(x_0 + d)$ is a better solution, so that $f(x_0 + d)$ is closer to zero. Equating it to zero gives

$$d = - \frac{f(x_0)}{df(x_0)/dx} \quad (57c)$$

That can be repeated until $f(x_0 + d)$ is close enough to zero. In Kepler's equation x is replaced by E and

$$f(E) = l - E + e \sin E = 0 \quad (58a)$$

$$\frac{df}{dE} = -1 - e \cos E \quad (58b)$$

Let E_0 be an approximation. Then $E_0 + d$ is a better one if

$$d = \frac{l - E_0 + e \sin E_0}{1 + e \cos E_0} \quad (59)$$

The iteration could well start from $E_0 = l$, but a closer guess is obtained by substituting this in Kepler's equation to get

$$E_0 = l + e \sin l \quad (60)$$

The iteration converges very rapidly and 3-5 steps give excellent precision. Other methods of solving the equations are given by Danby [1988], section 6.6.

The derivation of \mathbf{v} starts with

$$\mathbf{r} = r \cos f \hat{\xi} + r \sin f \hat{\eta} \quad (61)$$

Differentiate to get $\mathbf{v} = \frac{d\mathbf{r}}{dt}$

$$\mathbf{v} = \frac{dr}{dt} [\cos f \hat{\xi} + \sin f \hat{\eta}] + r \frac{df}{dt} [-\sin f \hat{\xi} + \cos f \hat{\eta}] \quad (62)$$

Now from the law of areas (29) and the ellipse (15)

$$r \frac{df}{dt} = \frac{h}{r} = \left[\frac{h}{p} \right] (1 + e \cos f) \quad (63a)$$

Also, differentiating (15) and substituting (29)

$$\frac{dr}{dt} = \frac{p}{(1 + e \cos f)^2} e \sin f \frac{df}{dt} = \frac{e \sin f}{p} r^2 \frac{df}{dt} = \frac{eh}{p} \sin f \quad (63b)$$

So

$$\mathbf{v} = \frac{eh}{p} \sin f [\cos f \hat{\xi} + \sin f \hat{\eta}] + \left[\frac{h}{p}\right] (1 + e \cos f) [-\sin f \hat{\xi} + \cos f \hat{\eta}] =$$

$$= \left[\frac{h}{p}\right] [\hat{\xi} \sin f [e \cos f - (1 + e \cos f)] + \hat{\eta} [e \sin^2 f + \cos f (1 + e \cos f)]]$$

or

$$\mathbf{v} = \left[\frac{h}{p}\right] [-\sin f \hat{\xi} + (e + \cos f) \hat{\eta}] \quad (64)$$

Both h and p depend on the orbit, but using (16), one of them can be eliminated, e.g.

$$h/p = (\mu/p)^{1/2} \quad (65)$$

4.3.2 Historical side excursion: Bessel functions

Bessel functions are named for an astronomer, not a mathematician. Friedrich Bessel lived in Germany in the early 1800s and devoted much of his career to accurate measurements of the positions of stars. His great discovery came in 1838, when he showed that during the year the position of one particular star shifted back and forth relative to its more distant neighbors, by a tiny amount, because the Earth viewed it from slightly different directions. That provided the first baseline for estimating the distances to the stars.

In 1824 (following earlier work in 1817) Bessel tried to solve Kepler's equation by a Fourier series:

$$E = l + \sum_{k=1}^{\infty} a_k \sin kl \quad (66)$$

In deriving this series for different orbits, the coefficients a_k will depend on the eccentricity e , but not on the semi-major axis a , because a has dimensions of length. In an equation for angles, a cannot appear alone, but only in the ratio to another length, and the equations contain no other quantity of that dimension.

As in the usual derivation of Fourier series, shift l to the left, multiply by $\sin(nl)$ and integrate from 0 to π

$$\int_0^{\pi} (E - l) \sin nl \, dl = \sum a_k \int_0^{\pi} \sin kl \sin nl \, dl = \frac{\pi}{2} a_n$$

The last equality holds because all right-hand integrals vanish unless $k = n$.

The integral on the left can be modified by integration by parts:

$$\int_0^{\pi} (E - l) \sin nl \, dl = -\frac{1}{n} \left[(E - l) \cos nl \right]_0^{\pi} + \frac{1}{n} \int_0^{\pi} \left(\frac{dE}{dl} - 1 \right) \cos nl \, dl$$

At $l = 0, \pi$, $(E - l) = 0$ and the first term vanishes, also $\int \cos nl \, dl = (1/n) \sin nl$ vanishes at the limits. Thus if $l = l(E)$

$$\frac{1}{n} \int_0^{\pi} \cos nl \, dE = \frac{\pi}{2} a_n$$

Substituting Kepler's equation

$$a_n(e) = \frac{2}{\pi n} \int_0^{\pi} \cos n(E - e \sin E) dE = \frac{2}{n} J_n(en) \quad (67)$$

That was how Bessel originally defined the Bessel function J_n . The definition looks unconventional, but Bessel's differential equation and series hold. See *Special Functions of Mathematical Physics and Chemistry* [Sneddon, 1961].

4.3.3 Given Initial Conditions

Often the orbital elements are not given, and instead one has the initial position \mathbf{r}_0 (in celestial coordinates) at $t=0$, and the initial velocity \mathbf{v}_0 .

To derive from this the first three orbital elements a , e , l_0 at $t=0$, the following method (following Battin [1968]) can be used. Start from

$$\mathbf{h} = \mathbf{r}_0 \times \mathbf{v}_0 \quad (11)$$

$$h = r_0^2 \frac{df_0}{dt} \quad (29)$$

$$r_0 = \frac{p}{1 + e \cos f_0} \quad (15)$$

Also, from (63b) and (16)

$$\frac{dr_0}{dt} = \frac{e\mu}{h} \sin f_0 \quad (68)$$

Since

$$\mathbf{v} = \frac{dr}{dt} \hat{\mathbf{r}} + r \frac{d\theta}{dt} \hat{\boldsymbol{\theta}} \quad (69)$$

the lhs of (68) can be expressed:

$$(\mathbf{v}_0 \cdot \mathbf{r}_0) = r_0 \frac{dr_0}{dt} = \frac{e\mu r_0}{h} \sin f_0 \quad (70)$$

Hence

$$e\mu \sin f_0 = \frac{h}{r_0} (\mathbf{v}_0 \cdot \mathbf{r}_0) \quad (71a)$$

and also from (15), above

$$e\mu \cos f_0 = \frac{h^2}{r_0} - \mu \quad (71b)$$

Squaring and adding given the equation for e

$$e^2 \mu^2 = \left(\frac{h}{r_0} \right)^2 (\mathbf{v}_0 \cdot \mathbf{r}_0)^2 + \left(\frac{h^2}{r_0} - \mu \right)^2 \quad (72)$$

once e is known, a can be derived, using (16) and (18)

$$p = \frac{h^2}{\mu} = a(1 - e^2) \quad (18)$$

Finally, (32) may be used to obtain $\cos E_0$:

$$r_0 = a(1 - e \cos E_0) \quad (32)$$

In the range $0 < E_0 < 2\pi$, $\cos E_0$ fits two values of E_0 --one in the lower half of the range, one in the upper one. The fact that f_0 is in the same half-range as E_0 determines which of these is used. Kepler's equation then gives l_0 as

$$l_0 = E_0 - e \sin E_0 \quad (51)$$

4.4 Motion in Three Dimensions

4.4.1 Celestial Coordinates

The basic frame of reference for all orbit calculations should be an **inertial** frame, one which does not rotate like frames associated with the Earth or the position of the Sun. Such a frame is provided by **celestial coordinates**, tied to the distant universe. At night the stars (except for the planets) appear to be attached to a huge sphere, the “celestial sphere”: in celestial coordinates, the position of each of them on that sphere is specified and fixed.

As the Earth rotates, the celestial sphere appears to revolve with a period close to 24 hours around two “*celestial poles*,” the points straight above the Earth’s own two poles. Stars close to the celestial poles seem to move in circles around them, and the closer the star, the smaller the circle: the “north star” moves in a very small circle around the north pole, though it is not exactly at it.

(Actually, the position of the poles slowly drifts, because the axis of the Earth in space is not fixed but rotates (“precesses”) around a cone, with a period of about 26,000 years. The Greeks already knew about this “precession of the equinoxes” but it will be ignored for now; it can be taken into account by correction terms in some of the equations.)

The period with which the celestial sphere (and all stars on it) appears to turn around its axis is about 4 minutes short of 24 hours: 24 hours is the average time the **Sun** goes around, but because the Earth orbits the Sun, the Sun appears to make one rotation less per year than the stars, making its average period a little longer.

A position on a sphere can be specified by spherical coordinates (θ, ϕ) . On the celestial sphere these are known as the **declination** δ and the **right ascension** α , respectively; right ascension is often measured in hours, minutes and seconds, and is measured from the “first point in Aries” (or “vernal equinox”) defined further below.

The quantities (δ, α) are generally called **celestial coordinates**, but **here** this term will also be applied to the **earth-centered rectangular coordinates** (x, y, z) corresponding to spherical (r, δ, α) . The celestial z axis points to the northern celestial pole, and the celestial x axis (see below) points to the first point in Aries.

4.4.2 The Ecliptic

The Earth moves around the Sun in a plane (see comment on eq. (11) above), known as the “**plane of the ecliptic**” or simply the ecliptic. From Earth we view that plane edge-on, and it appears to cut the celestial sphere into two halves, forming a big circle on it. The ecliptic is inclined by an angle $\epsilon \approx 23.45^\circ$ to the equatorial plane of the Earth, and that too is the angle at which that circle cuts the celestial equator.

Seen from Earth, the Sun must always be *somewhere* on that circle. The ancients identified 12 constellations of equal size around this circle, called the **zodiac**, since many are named after animals (“zoology” has a similar origin). As the Earth circles the Sun in the course of the year, the Sun appears to move around the circle and to spend a month in each constellation of the zodiac: of course, the constellation cannot be seen during that month, because the Sun’s brightness blots out its starlight.

In 3-dimensional space two non-parallel planes cut each other along a straight line, like the two parts of a hinge. The line along which the ecliptic intersects the equatorial plane of the Earth (i.e. the celestial equatorial plane) is chosen as the **celestial x-axis**.

Two directions are possible on that line, occupied by the Sun (as viewed from Earth) in spring and fall. The choice adopted is for the $+x$ direction to point towards the spring position (vernal equinox), the “first point in Aries”, so called because long ago it used to be in the constellation of Aries, the lamb. Because of the precession of the Earth’s axis (see above), it has gradually moved into Pisces (fish), and is now near the boundary between Pisces and Aquarius (the water carrier); that is the origin of the song “The dawning of the Age of Aquarius” in the musical play “Hair.”

4.4.3 Orbital Elements

The motion of a satellite is best defined in **orbital coordinates** (ξ, η, ζ) centered on Earth, with the (ξ, η) axes in the orbital plane and ξ along the long (major) axis of the orbital ellipse, pointing towards perigee. The **true anomaly** f (eq. (8) above) is thus the polar angle between the “radius vector” r and the ξ axis. The ζ axis, perpendicular to the orbital plane, will be assumed to extend into the **northern** celestial hemisphere.

The **orbital elements** are six numbers specifying the satellite’s position. **Three** of them give its position in the orbital plane, and the **other three** are angles specifying the position of that plane relative to the frame of celestial coordinates. The first three have already been discussed:

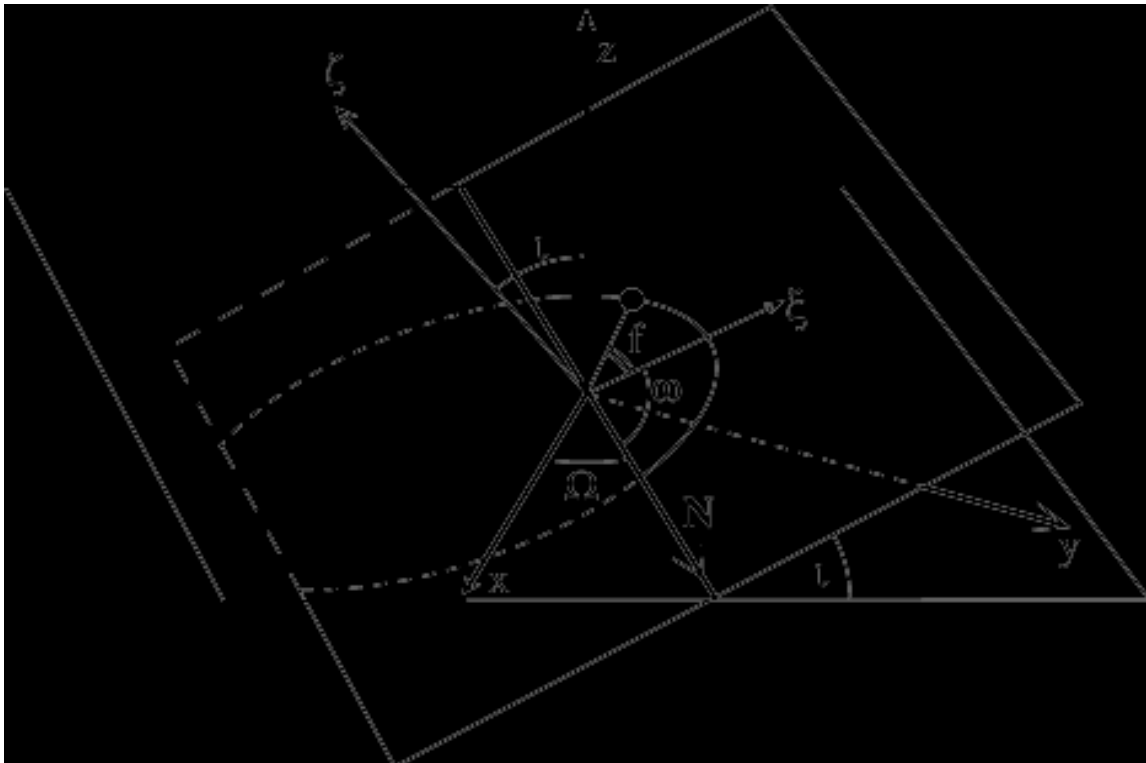
- (1) The **semi-major axis** a of the orbital ellipse.
- (2) The **eccentricity** e of the orbit.
- (3) The **mean anomaly** l , an angular measure increasing each orbit (like the true anomaly f) by 360° (or 2π radians), but linear in time.

The above three give the position along the orbit. In addition, **three angles**

(i, ω, Ω) specify the orbital plane itself and the orientation of the orbit inside it.

We assume that the orbital plane cuts the celestial equator (x, y) along the **line of nodes**, specified by the unit vector \mathbf{N} . The orbit itself cuts the line of nodes in two points, in one it enters the northern hemisphere, in the other it enters the southern hemisphere; \mathbf{N} is directed towards the *former* point. The angles then are

- (4) The **inclination** i of the orbital plane, i.e. the angle between the $\hat{\mathbf{z}}$ and $\hat{\boldsymbol{\xi}}$.



- (5) The **argument of perigee** ω , the angle between \mathbf{N} and the radius vector to perigee, i.e. the ξ axis (see drawing on previous page). It is measured in the (ξ, η) plane, the orbital plane.

- (6) The **longitude Ω of the ascending node**, the angle between **N** and the x axis, i.e. the direction to the first point in Aries (see Figure). It is measured in the (x, y) plane, the celestial equator.

4.4.4 Coordinate Transformations

To help relate orbital (ξ, η, ζ) to celestial (x, y, z) , two **auxiliary** systems of coordinates can be used, denoted here (x_n, y_n, z_n) and (x_i, y_i, z_i) .

Let $(\hat{x}, \hat{y}, \hat{z})$ and $(\hat{\xi}, \hat{\eta}, \hat{\zeta})$ be the respective unit vectors. In the orbital plane, the unit vector **N** along the line of nodes is given by

$$\mathbf{N} = \hat{\xi} \cos \omega - \hat{\eta} \sin \omega \quad (73)$$

The (x_n, y_n, z_n) coordinates are obtained by rotating (ξ, η, ζ) in the orbital plane so that $\hat{x} \rightarrow \hat{x}_n = \mathbf{N}$. Because the rotation is around the ζ axis, $z_n = \zeta$, unchanged. We get

$$\begin{pmatrix} x_n \\ y_n \\ z_n \end{pmatrix} = \begin{pmatrix} \cos \omega & -\sin \omega & 0 \\ \sin \omega & \cos \omega & 0 \\ 0 & 0 & 1 \end{pmatrix} \cdot \begin{pmatrix} \xi \\ \eta \\ \zeta \end{pmatrix} = \mathbf{A}_\omega \cdot \begin{pmatrix} \xi \\ \eta \\ \zeta \end{pmatrix} \quad (74)$$

Then

$$x_n = \xi \cos \omega - \eta \sin \omega \quad (75)$$

and applying the gradient operator recovers equation (13). Alternatively, one can start with unit vectors, define rotations and then infer corresponding relations such as (75). The latter approach was used here to derive rotations.

The next step consists of rotating the (x_n, y_n) plane by an angle i around the line of nodes, as if that line were a hinge, to the celestial equatorial plane. That produces the (x_i, y_i, z_i) system, with $\hat{x}_i = \hat{x}_n$ staying intact, since it lies along the line of nodes. From unit vectors

$$\begin{pmatrix} x_i \\ y_i \\ z_i \end{pmatrix} = \begin{pmatrix} 1 & 0 & 0 \\ 0 & \cos i & -\sin i \\ 0 & \sin i & \cos i \end{pmatrix} \cdot \begin{pmatrix} x_n \\ y_n \\ z_n \end{pmatrix} = \mathbf{A}_i \cdot \begin{pmatrix} x_n \\ y_n \\ z_n \end{pmatrix} \quad (76)$$

The z_i axis is now aligned with the celestial z axis, and only one more rotation is needed to align the other two coordinates with (x, y) , by the angle Ω which brings \hat{x}_i to the \hat{x} direction:

$$\begin{pmatrix} x \\ y \\ z \end{pmatrix} = \begin{pmatrix} \cos \Omega & -\sin \Omega & 0 \\ \sin \Omega & \cos \Omega & 0 \\ 0 & 0 & 1 \end{pmatrix} \cdot \begin{pmatrix} x_i \\ y_i \\ z_i \end{pmatrix} = \mathbf{A}_\Omega \cdot \begin{pmatrix} x_i \\ y_i \\ z_i \end{pmatrix} \quad (77)$$

By matrix multiplication

$$\begin{pmatrix} x \\ y \\ z \end{pmatrix} = \mathbf{A}_\Omega \cdot \mathbf{A}_i \cdot \mathbf{A}_\omega \cdot \begin{pmatrix} \xi \\ \eta \\ \zeta \end{pmatrix} = \mathbf{A} \cdot \begin{pmatrix} \xi \\ \eta \\ \zeta \end{pmatrix} \quad (78)$$

where **A** is given by

$$\cos \omega \cos \Omega - \cos i \sin \omega \sin \Omega \quad -\sin \omega \cos \Omega - \cos i \cos \omega \sin \Omega \quad \sin i \sin \Omega$$

$$\begin{array}{ccc} \cos\omega \sin\Omega + \cos i \sin\omega \cos\Omega & -\sin\omega \sin\Omega + \cos i \cos\omega \cos\Omega & -\sin i \cos\Omega \\ \sin i \sin\omega & \sin i \cos\omega & \cos i \end{array} \quad (79)$$

Note that \mathbf{A}_Ω , \mathbf{A}_i and \mathbf{A}_ω are hermitian, i.e. the transpose matrix obtained by flipping elements around the main diagonal gives the inverse transformation. Hence the same property also holds for \mathbf{A} .

4.4.5 Deriving the elements (i , ω , Ω) when $(\mathbf{r}_0, \mathbf{v}_0)$ are given

As shown in eqn (79), the above three angles give the matrix \mathbf{A} transforming orbital coordinates (ξ, η, ζ) to celestial ones (x, y, z) :

$$\begin{array}{c} x \\ y \\ z \end{array} = \mathbf{A} \cdot \begin{array}{c} \xi \\ \eta \\ \zeta \end{array} \quad (78)$$

However, it is also possible to derive \mathbf{A} directly from $(\mathbf{r}_0, \mathbf{v}_0)$ and use that information to determine the values of (i, ω, Ω) . To begin with, \mathbf{r}_0 and \mathbf{v}_0 are both in the orbital plane, hence their vector product is orthogonal to that plane and by definition gives $\hat{\zeta}$:

$$\hat{\zeta} = \frac{\mathbf{r}_0 \times \mathbf{v}_0}{\|\mathbf{r}_0 \times \mathbf{v}_0\|} \quad (80)$$

Since \mathbf{A} is hermitian:

$$\begin{array}{c} \xi \\ \eta \\ \zeta \end{array} = \mathbf{A}^T \cdot \begin{array}{c} x \\ y \\ z \end{array} \quad (81)$$

it follows that

$$\hat{\zeta} = A_{13} \hat{x} + A_{23} \hat{y} + A_{33} \hat{z} \quad (82)$$

Since the inclination i is the angle between $\hat{\zeta}$ and \hat{z}

$$\hat{\zeta} \cdot \hat{z} = \cos i = A_{33} \quad (83)$$

which also agrees with (79); since the inclination i is limited to the range $0 < i < \pi$, the above defines $\sin i$ as well.

In the orbital plane, $\hat{\mathbf{r}}_0 = \mathbf{r}_0/r_0$ and $\hat{\mathbf{r}}_0 \times \hat{\zeta}$ are two orthogonal unit vectors, making angles f_0 and $\pi/2 - f_0$ with the ξ -direction (see drawing). Hence

$$\begin{aligned} \hat{\zeta} &= \hat{\mathbf{r}}_0 \cos f_0 + (\hat{\mathbf{r}}_0 \times \hat{\zeta}) \sin f_0 \\ &= A_{11} \hat{x} + A_{21} \hat{y} + A_{31} \hat{z} \end{aligned} \quad (84)$$

Here the functions of f_0 are given by (71), the celestial components of \mathbf{r}_0 are part of the input and those of $(\hat{\mathbf{r}}_0 \times \hat{\zeta})$ are easily obtained from (80), giving another column of \mathbf{A} . Finally

$$\hat{\eta} = (\hat{\zeta} \times \hat{\xi}) = \hat{\mathbf{r}}_0 \sin f_0 - (\hat{\mathbf{r}}_0 \times \hat{\zeta}) \cos f_0 \quad (85)$$

gives the middle column.

When the matrix (79) is equated to \mathbf{A} as derived here, we get 9 scalar equations, from which in principle ω and Ω can be derived (i is already known from (83)). The algebra is greatly simplified, however, if one notes that by (78), \mathbf{A} is the product of three hermitian matrices

$$\mathbf{A} = \mathbf{A}_\Omega \cdot \mathbf{A}_i \cdot \mathbf{A}_\omega$$

and hence

$$\mathbf{A} \cdot \mathbf{A}_\omega^T = \mathbf{A}_\Omega \cdot \mathbf{A}_i \quad (86)$$

Spelled out:

$$\begin{array}{ccc|ccc} A_{11} & A_{12} & A_{13} & \cos\omega & \sin\omega & 0 \\ A_{21} & A_{22} & A_{23} & -\sin\omega & \cos\omega & 0 \\ A_{31} & A_{32} & A_{33} & 0 & 0 & 1 \end{array} = \begin{array}{ccc} \cos\Omega & -\sin\Omega \cos i & \sin\Omega \sin i \\ \sin\Omega & \cos\Omega \cos i & -\cos\Omega \sin i \\ 0 & \sin i & \cos i \end{array} \quad (87)$$

The factorization gives nine equations:

$$A_{11} \cos\omega - A_{12} \sin\omega = \cos\Omega \quad (88-1)$$

$$A_{21} \cos\omega - A_{22} \sin\omega = \sin\Omega \quad (88-2)$$

$$A_{31} \cos\omega - A_{32} \sin\omega = 0 \quad (88-3)$$

$$A_{11} \sin\omega + A_{12} \cos\omega = -\cos i \sin\Omega \quad (88-4)$$

$$A_{21} \sin\omega + A_{22} \cos\omega = \cos i \cos\Omega \quad (88-5)$$

$$A_{31} \sin\omega + A_{32} \cos\omega = \sin i \quad (88-6)$$

$$A_{13} = \sin\Omega \sin i \quad (88-7)$$

$$A_{23} = \cos\Omega \sin i \quad (88-8)$$

$$A_{33} = \cos i \quad (88-9)$$

With 9 equations defining 3 unknown angles, extracting those angles seems like an easy task, but care is needed, because the equations are not independent. Furthermore, since either $\sin i$ or $\cos i$ can go through zero, it is best to avoid division by those factors. Starting with (88-9)

$$\cos i = A_{33} \quad (88-9)$$

Then by (88-3)

$$A_{32}^2 \sin^2\omega = A_{31}^2 \cos^2\omega = A_{31}^2 (1 - \sin^2\omega)$$

$$\sin\omega = \pm A_{31} / (A_{31}^2 + A_{32}^2)^{1/2} \quad (89a)$$

Since we do not yet know the proper sign, we assume temporarily $\sin\omega > 0$:

$$\sin\omega = A_{31} / (A_{31}^2 + A_{32}^2)^{1/2} \quad (89b)$$

Then by (88-3)

$$\cos\omega = A_{32} / (A_{31}^2 + A_{32}^2)^{1/2} \quad (89c)$$

And by (88-6)

$$A_{31} \sin\omega + A_{32} \cos\omega = \sin i$$

The angle i is between 0° and 180° , hence $\sin i > 0$. If then equation (88-6) gives it a negative value, this means the signs of $(\sin\omega, \cos\omega)$ must be reversed. If $\sin i = 0$, the situation is degenerate, no line of nodes is defined, and (ω, Ω) are ill-defined too; only their sum $\omega + \Omega$ has any meaning.

Suppose the ζ -axis moves through the z -axis, approaching it from one side and then receding on the opposite side. The inclination i decreases to zero and ζ and z coincide, but after that it does not

cross into negative i as might be naively assumed, but rather, bounces back into the positive range, possibly with a discontinuous slope, because the range of i is 0^0 to 180^0 . What *does* happen however is that ω and Ω jump by 180^0 as the ascending node and the descending node switch sides. The same orbit but clockwise would have inclinations around 180^0

Now equations (88-1) and (88-2) give $(\cos\Omega, \sin\Omega)$, completing the set. Nowhere has it been necessary to divide by $\sin i$ or by $\cos i$.

4.5 Transformations that depend on the Time

4.5.1 Relating (x,y,z) to geographic coordinates.

The frame of celestial coordinates (x,y,z) is inertial, fixed in space. The Earth has its own frame of reference, its geographic coordinates (x_g, y_g, z_g). Because the Earth rotates, the relation between the two is time-dependent, and to express it properly, some system of measuring time must be specified. The system preferred here is that of **Julian time**.

4.5.2 Julian Time

Any astronomical calculations that depend on time require some standard system of time measurements. Traditionally astronomers use the **Julian Day** or Julian date (JD), with fractions denoting the part of the day that has elapsed.

There is a problem in matching the fractional part, though, because the commonly used measure for fractions of day, **universal time** (UT) is measured from **midnight**. (Astronomers also call it "Greenwich civil time," while they reckon "Greenwich Mean Time" or GMT from noon.)

On the other hand, the Julian day by tradition starts at **noon**. Then on any day at $UT = 0$ the Julian time is a half-integral number, ending in .5

The usual method of calculating Julian time is therefore to use the sum of the Julian time at $UT = 0$, a half-integral number, and add to it the UT, as a fraction of a day. The result will be denoted as the **Julian Day**, since it is measured in days.

Below is the algorithm used by Meeus [1991] to calculate the Julian day JD for epoch J2000.0 at universal time UT in year Y, month M, day D (with fractional part). M should be between 3 to 14, so that if $M=1,2$, a year is changed into months ($Y \rightarrow Y-1, M \rightarrow M+12$). Then

$$\begin{aligned} A &= \text{INT}(Y/100) & (= \text{century no.}) \\ B &= 2 - A + \text{INT}(A/4) \end{aligned}$$

Then the Julian Day JD is

$$JD = \text{INT}[365.25(Y + 4716)] + \text{INT}[30.6001(M+1)] + D + B - 1524.5$$

Note that on (say) 0 UT on April 10, $D=10$, even though only 9 days have elapsed since the beginning of the month: this avoids having a "day zero" in each month, and is all accommodated by the constant added.

The value of JD is in the millions, so actual formulas introduce a measure of time given by a smaller number, the **epoch time T** in Julian centuries

$$T = \frac{JD - 2451\,545.0}{36525} \quad (90)$$

4.5.3 The Earth's Rotation

The amount of rotation which the Earth has undergone at any given UT is given by the angle ϕ_g at that time, the angle between the celestial x direction and the geographic x_g direction, which is on the Greenwich meridian. For

UT = 0 on any day (i.e. with JD in (90) a half-integral number), ϕ_g in (hrs, min, sec) is given by

$$\phi_g = 6^h 41^m 50^s.54841 + 8640 184^s .812866 T + 0^s.093 104 T^2 - 0^s.000 0062 T^3 \quad (91)$$

or in degrees

$$\phi_g = 100.460 618 37 + 36 000.770 053 608 T + 0.000 387 933 T^2 - T^3/38 710 000 \quad (92)$$

The nonlinear terms presumably express the slowing down of the Earth's rotation.

To find ϕ_g for any other UT, multiply UT (in degrees, $24 \text{ h} = 360^\circ$) by 1.002 737 909 35 ($\approx 1 + 1/365.25$) and add. Thus ϕ_g rotates each day a little over a full circle. Or else, given JD with fractional value, one calculates

$$\phi_g = 280.460 618 37 + 360.985647 366 29 (\text{JD} - 2451 545.0) + 0.000 387 933 T^2 - T^3/38 710 000 \quad (93)$$

It is however better to treat UT separately, otherwise accuracy may be lost in (90), where two nearly equal numbers are subtracted. In any case, double-precision calculations are pretty much indicated in all such work.

4.5.4 Relating geographic and celestial coordinates

The two are related by a rotation by the angle ϕ_g :

$$\begin{aligned} x_g &= x \cos\phi_g + y \sin\phi_g \\ y_g &= -x \sin\phi_g + y \cos\phi_g \\ z_g &= z \end{aligned} \quad (94a)$$

hence

$$\begin{pmatrix} x_g \\ y_g \\ z_g \end{pmatrix} = \mathbf{A}_2 \cdot \begin{pmatrix} x \\ y \\ z \end{pmatrix} \quad (94b)$$

where

$$\mathbf{A}_2 = \begin{pmatrix} \cos\phi_g & \sin\phi_g & 0 \\ -\sin\phi_g & \cos\phi_g & 0 \\ 0 & 0 & 1 \end{pmatrix} \quad (94c)$$

4.5.5 Ecliptic Coordinates ("celestial" in Meeus)

The first step in deriving the position of the Sun is a rotation to ecliptic coordinates (x_e, y_e, z_e) , with the x_e -axis as before pointing to the first point in Aries but the z -axis rotated by an angle $\epsilon \approx 23.45^\circ$ around the x -axis:

$$\begin{aligned} x_e &= x \\ y_e &= y \cos\epsilon - z \sin\epsilon \\ z_e &= y \sin\epsilon + z \cos\epsilon \end{aligned} \quad (95a)$$

hence

$$\begin{pmatrix} x_e \\ y_e \\ z_e \end{pmatrix} = \mathbf{A}_3 \cdot \begin{pmatrix} x \\ y \\ z \end{pmatrix} \quad (95b)$$

with

$$\mathbf{A}_3 = \begin{pmatrix} 1 & 0 & 0 \\ 0 & \cos\epsilon & -\sin\epsilon \\ 0 & \sin\epsilon & \cos\epsilon \end{pmatrix} \quad (95c)$$

4.5.6 The position of the Sun

Finally, we need the **vector pointing at the Sun**.

If λ is the ecliptic longitude of the Sun (its "celestial longitude" in Meeus, p. 87.7), then the unit vector to the Sun is

$$\hat{\mathbf{r}}_s = \hat{\mathbf{x}}_e \cos\lambda + \hat{\mathbf{y}}_e \sin\lambda \quad (96)$$

Given below are two derivations of λ : that of "low precision formulas for positions of Sun and Moon" of the nautical almanac, and the derivation by Meeus [1991] of the "true longitude" Θ which differs from λ by some seconds of arc (the book also gives a more accurate derivation of λ).

The position of the Sun is needed for two purposes, to obtain the approximate direction of the solar wind for modeling the magnetosphere, and to derive the Sun's perturbation of a satellite orbit. Since the direction of the solar wind fluctuates by several degrees and the perturbation term is merely a small correction to the equations of motion, low accuracy formulas are quite adequate.

Below the notation of the astronomical almanac is retained. The time parameter is

$$n = \text{JD} - 2\,451\,545.0 \quad (97)$$

The mean longitude of the Sun, corrected for aberration, is then

$$L = 280.461 + 0.985\,6474\,n \quad (98)$$

Mean anomaly, in degrees

$$g = 357.528 + 0.9856003\,n \quad (99)$$

Ecliptic longitude, in degrees

$$\lambda = L + 1.915 \sin g + 0.020 \sin 2g \quad (100)$$

Angle between the ecliptic and the equator, in degrees

$$\varepsilon = 23.439 - 0.000\,0004\,n \quad (101)$$

Distance R to the Sun, in AU, where 1 AU = $1.49599 \cdot 10^{11}$ m

$$R = 1.000\,14 - 0.016\,71 \cos g - 0.000\,14 \cos 2g \quad (102)$$

In Meeus [1991] on p. 151, the time parameter is $T = n/36525$, i.e. where n is in Julian days, T is in Julian centuries. Then

$$L = 280.46645 + 36000.76983\,T + 0.0003032\,T^2 \quad (103a)$$

$$M = 357.5290 + 35999.05030\,T - 0.000\,1559\,T^2 - 0.000\,000\,48\,T^3 \quad (103b)$$

and the “true longitude” is

$$\begin{aligned} \Theta = L &+ (1.914600 - 0.004\,817\,T - 0.000\,014\,T^2) \sin M \\ &+ (0.019\,993 - 0.000\,101\,T) \sin 2M + 0.000\,290 \sin 3M \end{aligned} \quad (104)$$

Meeus also gives a formula for ε in degrees, minutes and seconds, to order T^3
Finally

$$R = 1.000\,01018 (1 - e^2)/1 + e \cos v \quad (105)$$

where v is the true anomaly $v = M + (\Theta - L)$

4.5.7 Solar ecliptic coordinates

These coordinates, denoted (x_s, y_s, z_s) , are defined as having $z_s = z_e$ but with x_s pointing at the Sun

$$\begin{aligned} x_s &= x_e \cos \lambda + y_e \sin \lambda \\ y_s &= -x_e \sin \lambda + y_e \cos \lambda \\ z_s &= z_e \end{aligned} \quad (106a)$$

$$\begin{pmatrix} x_s \\ y_s \\ z_s \end{pmatrix} = \mathbf{A}_4 \cdot \begin{pmatrix} x_e \\ y_e \\ z_e \end{pmatrix} \quad (106b)$$

4.6 The Earth's Magnetic Field

The Earth's magnetic field can be approximated by a magnetic dipole at the Earth's center, inclined by an angle $\theta_0 \approx 11.2^\circ$ to the Earth's rotation axis, along the meridian $\phi = \phi_0 \approx -70.75^\circ$ where $\phi = 0$ is the Greenwich meridian. To accurately describe the global field, especially near the Earth's surface, additional magnetic field components must be added, usually expressed by the gradient of a scalar magnetic potential, expanded in spherical harmonics. For best fit to this corrected magnetic field, the dipole representing the field must be slightly shifted from the center of the Earth. However, all these corrections are relatively small at $r > 5 R_E$ and are completely negligible for $r > 10 R_E$; since the "Profile" mission is primarily concerned with the distant field, they will be neglected.

4.6.1 Dipole Coordinates

Let (x_g, y_g, z_g) be **geographic** coordinates-- z_g along the Earth's axis, x_g through the Greenwich meridian. The dipole axis passes the magnetic pole at $(\theta_d, \phi_d) = (11.2^\circ, -70.75^\circ)$. The northward unit vector along that axis is

$$\hat{\mathbf{z}}_d = \hat{\rho}_g \sin\theta_0 + \hat{\mathbf{z}}_g \cos\theta_0 \quad (107a)$$

where

$$\hat{\rho}_g = \hat{\mathbf{x}}_g \cos\phi_0 + \hat{\mathbf{y}}_g \sin\phi_0 \quad (107b)$$

hence

$$\hat{\mathbf{z}}_d = \hat{\mathbf{x}}_g \sin\theta_0 \cos\phi_0 + \hat{\mathbf{y}}_g \sin\theta_0 \sin\phi_0 + \hat{\mathbf{z}}_g \cos\theta_0 \quad (107c)$$

The x_d axis is in the same plane as z_d and z_g , hence y_d is normal to that plane, and it follows (for a right-hand system)

$$\hat{\mathbf{y}}_d = \frac{\hat{\mathbf{z}}_g \times \hat{\mathbf{z}}_d}{\|\hat{\mathbf{z}}_g \times \hat{\mathbf{z}}_d\|} \quad (108)$$

Now

$$\hat{\mathbf{z}}_g \times \hat{\mathbf{z}}_d = -\hat{\mathbf{x}}_g \sin\theta_0 \sin\phi_0 + \hat{\mathbf{y}}_g \sin\theta_0 \cos\phi_0$$

and the magnitude of that vector is $\sin\theta_0$, hence

$$\hat{\mathbf{y}}_d = -\hat{\mathbf{x}}_g \sin\phi_0 + \hat{\mathbf{y}}_g \cos\phi_0 \quad (109)$$

Finally

$$\hat{\mathbf{x}}_d = \hat{\mathbf{y}}_d \times \hat{\mathbf{z}}_d = \hat{\mathbf{x}}_g \cos\theta_0 \cos\phi_0 + \hat{\mathbf{y}}_g \cos\theta_0 \sin\phi_0 - \hat{\mathbf{z}}_g \sin\theta_0 \quad (110)$$

We thus find that the rotation, between either unit vectors or coordinates, involves a matrix \mathbf{A}_1 satisfying

$$\begin{pmatrix} x_d \\ y_d \\ z_d \end{pmatrix} = \mathbf{A}_1 \cdot \begin{pmatrix} x_g \\ y_g \\ z_g \end{pmatrix} \quad (111)$$

where

$$\mathbf{A}_1 = \begin{pmatrix} \cos\theta_0 \cos\phi_0 & \cos\theta_0 \sin\phi_0 & -\sin\theta_0 \\ -\sin\phi_0 & \cos\phi_0 & 0 \\ \sin\theta_0 \cos\phi_0 & \sin\theta_0 \sin\phi_0 & \cos\theta_0 \end{pmatrix} \quad (112)$$

\mathbf{A}_1 is of course hermitian, $\mathbf{A}_1^{-1} = \mathbf{A}_1^T$.

4.6.2 Locating the Magnetic Pole

The dipole field can be expressed by

$$\begin{aligned}
 \mathbf{B} &= -\nabla\gamma_0 = -a \nabla[g_1^0 \cos\theta + g_1^1 \sin\theta \cos\phi + h_1^1 \sin\theta \sin\phi] (a/r)^2 \\
 &= -\nabla (g_1^0 z_g + g_1^1 x_g + h_1^1 y_g) (a/r)^3 \\
 &= -(g_1^0 \hat{\mathbf{z}}_g + g_1^1 \hat{\mathbf{x}}_g + h_1^1 \hat{\mathbf{y}}_g) (a/r)^3 + \hat{\mathbf{r}} f(r)
 \end{aligned} \tag{113}$$

(no subscript on r , which is the same in all earth-centered systems).

On the dipole axis \mathbf{B} is radial. Neglecting the sign for a moment,

$$\begin{aligned}
 (g_1^0 \hat{\mathbf{z}}_g + g_1^1 \hat{\mathbf{x}}_g + h_1^1 \hat{\mathbf{y}}_g) &= k \hat{\mathbf{r}} \\
 &= k [\hat{\mathbf{x}}_g \sin\theta_0 \cos\phi_0 + \hat{\mathbf{y}}_g \sin\theta_0 \sin\phi_0 + \hat{\mathbf{z}}_g \cos\theta_0]
 \end{aligned} \tag{114}$$

Comparing magnitudes of the two vectors

$$k^2 = (g_1^0)^2 + (g_1^1)^2 + (h_1^1)^2 \tag{115}$$

Equating terms then gives

$$\begin{aligned}
 \cos\theta_0 &= g_1^0/k \\
 \sin\phi_0 &= h_1^1/k\sin\theta_0
 \end{aligned} \tag{116}$$

and to resolve ambiguity (in case signs need to be inverted)

$$\cos\phi_0 = g_1^1/k\sin\theta_0$$

4.7 The Earth's Magnetosphere and its Coordinate System

4.7.1 The Configuration of the Magnetosphere

Most of the magnetosphere is filled with a nearly collision-free plasma, and its electrodynamic properties therefore tend to spread along magnetic field lines. We will thus count as belonging to the magnetosphere all points in space linked to Earth by magnetic field lines. Near Earth these lines are "closed," i.e. anchored in Earth at both their ends. In addition, some lines connected to the polar caps appear to be "open," i.e. temporarily linked to interplanetary field lines, though in practice it is in general not easy to trace where that linkage occurs. A third class of field lines are those of the interplanetary magnetic field (IMF) which are embedded in the solar wind and travel with it.

The IMF and the solar wind confine the field lines of the magnetosphere inside a cavity, bullet-shaped in front and tending to a cylinder on the night side. The surface separating it from the magnetosphere is known as the magnetopause: in observations it is usually marked by a sudden shift of the magnetic field \mathbf{B} and the plasma density n . However, the component B_n normal to the magnetopause is generally small and in the presence of noise it is not easy to tell when it is small but finite (as expected from open lines) and when zero.

On the dayside, the "subsolar distance" r_s of the "nose" of the magnetosphere from the center of Earth is typically $10\text{--}11 R_E$, the distance to the boundary abreast of Earth is about $15 R_E$ and the asymptotic radius of the distant tail is about $25\text{--}30 R_E$. These and other parameters defining the magnetosphere can change appreciably, depending on the solar wind pressure, the IMF and the preceding history of magnetic activity. Sunward of the magnetopause is the collisionless bow shock, typically $2\text{--}3 R_E$ beyond the "nose." Outside the bow shock is the solar wind, while behind it is the magnetosheath, plasma which has passed through the shock, where it has heated up at the expense of its bulk velocity. That velocity gradually recovers its interplanetary value as the plasma flows past the Earth.

Of the magnetic field lines swept into the tail, most extend beyond the range of regular observations and form two oppositely directed bundles, the *tail lobes*. Separating the two lobes is a region of very stretched but closed field lines known as the *plasma sheet*, because its plasma density (typically 0.4 ions/cm^3) is much higher than that of the lobes. Typically the plasma sheet is $2\text{--}6 R_E$ thick and its central surface, the locus of minimum $|\mathbf{B}|$ on the threading field lines, is known as the *neutral sheet*.

Schematic drawings of the magnetosphere often show a dipole axis perpendicular to the direction of the solar wind. However, the actual angle between the two varies, because of the inclination $\epsilon = 23.45^\circ$ of the Earth axis, combined with the offset angle $\phi_0 = 11.2^\circ$ between the magnetic dipole and the rotation axis.

It is customary to express these effects by means of the *tilt angle* ψ which complements to 90° the angle between the dipole axis and the vector pointing into the flow of the solar wind, i.e. $\psi = 0^\circ$ signifies a dipole axis perpendicular to the solar wind. The actual solar value of ψ varies with time between the limits $\pm(\epsilon + \phi_0) \approx \pm 34.65^\circ$.

The equatorial surface of the magnetosphere, which includes the neutral sheet, also varies with ψ , as described further below.

4.7.2 Geocentric solar magnetospheric coordinates

Suppose the unit vector $\hat{\mathbf{z}}_d$ along the dipole axis makes an angle $90^\circ - \psi$ with the unit vector $\hat{\mathbf{x}}_s$ pointing to the Sun, which is also assumed to be the direction from which the solar wind arrives. Neglecting all non-dipole components of the Earth's field and any effects of the IMF, only two vectors affect the geometry of the magnetosphere, namely $\hat{\mathbf{x}}_s$ and $\hat{\mathbf{z}}_d$. One therefore expects the plane of those two vectors to be a plane of symmetry of the magnetosphere.

If the magnetic dipole were exactly aligned with the Earth's rotation axis, i.e. if θ_0 in (98) were zero, that plane would rock back and forth around the x_s axis in an annual cycle, aligning itself with the (x_s, z_s) plane at the solstices and departing from it the most at the equinoxes. Because $\phi_0 \neq 0$, the plane of (\hat{x}_s, \hat{z}_d) undergoes on top of the above variation an additional back-and-forth rocking motion of smaller amplitude and with a period of 24 hours.

The **geocentric solar magnetospheric (gsm)** system of coordinates (x_{sm}, y_{sm}, z_{sm}) has this plane of symmetry as its (x_{sm}, z_{sm}) plane, with x_{sm} along the Earth-to-Sun direction, i.e. $x_{sm} = x_s$. Thus gsm coordinates are obtained by rotating the solar ecliptic coordinates by some angle χ around the x_s axis:

$$\begin{aligned} x_{sm} &= x_s \\ y_{sm} &= y_s \cos \chi - z_s \sin \chi \\ z_{sm} &= y_s \sin \chi + z_s \cos \chi \end{aligned} \quad (117a)$$

From this

$$\mathbf{r}_{sm} = \mathbf{A}_5 \cdot \mathbf{r}_s \quad (117b)$$

with

$$\mathbf{A}_5 = \begin{pmatrix} 1 & 0 & 0 \\ 0 & \cos \chi & -\sin \chi \\ 0 & \sin \chi & \cos \chi \end{pmatrix} \quad (117c)$$

To obtain χ it is necessary to retrace transformations from solar ecliptic through ecliptic, celestial and geographic, all the way to dipole coordinates, and express in the solar-ecliptic frame the unit vector $\hat{\mathbf{z}}_d$ along the dipole axis:

$$\hat{\mathbf{z}}_d = a \hat{\mathbf{x}}_s + b \hat{\mathbf{y}}_s + c \hat{\mathbf{z}}_s \quad (118a)$$

We also know that

$$\hat{\mathbf{z}}_d = \hat{\mathbf{x}}_{sm} \sin \psi + \hat{\mathbf{z}}_{sm} \cos \psi \quad (118b)$$

Since $\hat{\mathbf{x}}_{sm} = \hat{\mathbf{x}}_s$, comparing the above two equations gives

$$\sin \psi = a \quad (119a)$$

$$\hat{\mathbf{z}}_{sm} \cos \psi = b \hat{\mathbf{z}}_s + c \hat{\mathbf{z}}_s \quad (119b)$$

and since $\hat{\mathbf{z}}_{sm}$ is a unit vector

$$\hat{\mathbf{z}}_{sm} = (b^2 + c^2)^{-1/2} [b \hat{\mathbf{z}}_s + c \hat{\mathbf{z}}_s] \quad (120)$$

from which, by (116)

$$\sin \chi = \frac{c}{(b^2 + c^2)^{1/2}} \quad \cos \chi = \frac{b}{(b^2 + c^2)^{1/2}} \quad \tan \chi = \frac{b}{c} \quad (121)$$

4.7.3 Aberrated GSM coordinates (AGSM)

For an observer in the Earth's frame, the direction from which the solar wind appears to blow is not that of $\hat{\mathbf{x}}_s$, but one that is aberrated by an angle $\phi_a \approx 4^\circ$ due to the Earth's motion around the Sun. To take that effect into account in derivations like the one above, it is necessary to replace the ecliptic coordinates $(x_s,$

y_s, z_s) by aberrated coordinates (x_a, y_a, z_a) , obtained by rotating the ecliptic coordinates by an angle ϕ_a around the z_s axis:

$$\begin{pmatrix} x_a \\ y_a \\ z_a \end{pmatrix} = \begin{pmatrix} \cos \phi_a & -\sin \phi_a & 0 \\ \sin \phi_a & \cos \phi_a & 0 \\ 0 & 0 & 1 \end{pmatrix} \begin{pmatrix} x_s \\ y_s \\ z_s \end{pmatrix} \quad (122)$$

This correction was not included in any of the calculations here, since it is small and since the direction from which the solar wind arrives at Earth undergoes in addition a random variation of comparable magnitude.

4.7.4 Sequence of calculations

Start with eq. (109c) for the unit vector along the dipole axis in geographic coordinates.

$$\hat{\mathbf{z}}_d = \hat{\mathbf{x}}_g \sin \theta_0 \cos \phi_0 + \hat{\mathbf{y}}_g \sin \theta_0 \sin \phi_0 + \hat{\mathbf{z}}_g \cos \theta_0 \quad (107c)$$

Let this vector be denoted \mathbf{r}_g for brevity, since it is in geographic coordinates. transforming to celestial coords., by (94)

$$\hat{\mathbf{r}} = \mathbf{A}_2^{-1} \hat{\mathbf{r}}_g$$

In ecliptic coords., by (95)

$$\hat{\mathbf{r}}_e = \mathbf{A}_3 \mathbf{A}_2^{-1} \hat{\mathbf{r}}_g$$

and reaching solar ecliptic coords, by (96), (118)

$$\hat{\mathbf{r}}_s = \mathbf{A}_4 \mathbf{A}_3 \mathbf{A}_2^{-1} \hat{\mathbf{r}}_g = a \hat{\mathbf{x}}_s + b \hat{\mathbf{y}}_s + c \hat{\mathbf{z}}_s \quad (123)$$

$$\text{Then if } \text{PMG} = \text{SQRT}(b^2 + c^2) \quad \sin \psi = b/\text{PMG} \quad \cos \psi = c/\text{PMG}$$

Next suppose the celestial coordinates of some orbital point $\mathbf{R} = (x, y, z)$ are given. To obtain the GSM components \mathbf{R}_{sm} , we need derive

$$\mathbf{R}_{sm} = (\mathbf{A}_5 \mathbf{A}_4 \mathbf{A}_3) \mathbf{R} \quad (124)$$

This suggests a need for two further matrices:

$$\mathbf{A}_6 = \mathbf{A}_4 \mathbf{A}_3 \mathbf{A}_2^{-1} \quad [\text{used in (121) above}] \quad (125a)$$

and

$$\mathbf{A}_7 = \mathbf{A}_5 \mathbf{A}_4 \mathbf{A}_3 \quad (125b)$$

from which

$$\mathbf{r}_{smc} = \mathbf{A}_7 \cdot \mathbf{r} \quad (125c)$$

4.8 Regions of the Magnetosphere

Given all the orbital mechanics and coordinate transformations, it is possible to simulate “Profile” missions and in particular, find how effectively their multi-spacecraft constellations sample various regions of the magnetosphere. The position of any given orbit in the magnetosphere is far from static: not only does it rotate around the Earth (in GSM coordinates) during the course of a year, but the tilt angle also modifies the structure of the field. In addition, of course, changes occur which can’t be predicted, e.g. those due to varying solar wind pressure and activity levels.

The Space Situation Center (SSC) which tracks spacecraft orbits for the National Space Science Data Center (NSSDC) has a code, written by Mauricio Peredo, classifying any point in space according to the magnetospheric region it is most likely to occupy. Its description is found on the world Wide Web at

http://sscopl.gsfc.nasa.gov/ssc_reg_doc.html

That code is rather lengthy and was therefore not used here, though some of its formulas were retained. Instead, a customized code was written, addressing the particular needs of "Profile." In its current form, that code assigns to the point which is being examined an index IREG from 0 to 9, classifying it as belonging to one of the following categories:

- IREG = 0 Inner magnetosphere
- = 1 Near the magnetopause, probably inside it.
 - = 2 Near the magnetopause, probably outside it
 - = 3 Outside magnetopause, but inside the bow shock
 - = 4 Solar wind, outside the bow shock
 - = 5 Tail lobe
 - = 6 Probably in the plasma sheet
 - = 7 Near center of plasma sheet.
 - = 8 Transition between inner magnetosphere and plasma sheet.
 - = 9 cusp or polar region on the day side

The preceding drawing sketches out these regions in the z_{sm} plane. It must be stressed here that the classifications merely state high likelihood of the point belonging to a region, for average solar wind conditions. The code which classifies points contains three algorithms, similar to those used in the SSC code:

- (1) An analytical approximation to the shape of the **magnetopause**, due to [Sibeck et al.](#) (JGR 96, 5489, 1991)
- (2) An analytical approximation to the shape of the **bow shock**, based on one by [Fairfield](#) (JGR 76, 6700, 1971).
- (3) An analytical approximation to the shape of the **equatorial surface**, based on one by [Tsyganenko](#) (JGR 100, 5599, 1995, eqs. 24-26).

4.8.1 The Magnetopause

[Sibeck et al.](#) [1991] approximated the shape of the magnetopause by an axisymmetric surface. If in GSM (or in aberrated AGSM)

$$R^2 = y^2 + z^2 \quad (126a)$$

then the magnetopause is approximated by an ellipsoid

$$F_1(\mathbf{r}) = R^2 + S_1 x^2 + S_2 (p/p_0)^{1/6} x + S_3 (p/p_0)^{1/3} = 0 \quad (126b)$$

where p is the solar wind dynamic pressure, with $p_0 = 2.04$ its average value, $S_1 = 0.14$, $S_2 = 18.2$, $S_3 = -217.2$, and where all distances are in units of the Earth radius R_E . In simulating the mission we assume $p = p_0$ and neglect the factors with p/p_0 , but they might come useful in later work. Eq. (126b) also ignores the effects of the interplanetary magnetic field, whose effects were also studied in that article and in later work by the same authors.

The distance r_s of the **subsolar point** (“nose of the magnetosphere”) is obtained by solving for $R=0$: it is very close to $11 R_E$.

For the regions characterized by IREG=1 and 2 we next seek two additional ellipsoids enclosing the surface, one on the inside, one on the outside, cutting the x -axis at $r_s \pm 1 R_E$. It would be easy to define such surfaces by scaling all distances in (126) by the appropriate factor k , in a way similar to what is done for the bow shock in the next section, giving ellipsoids of the same shape but different scales. That however causes the ellipsoids to be most widely spaced at the subsolar point, whereas the boundary layers, for instance, are narrowest there.

Instead, therefore, we choose the two other ellipses to have the **same foci** as the one of (126b), making the spacing smallest at the subsolar point. If the factor (p/p_0) in (126b) is ignored (i.e. is equal to 1; it can easily be reinstated) and

$$A = S_1 \quad B = S_2/2S_1 \quad C = S_3 - S_2^2/4S_1$$

then

$$F_1(\mathbf{r}) = R^2 + A^2(x+B)^2 = C \quad (127a)$$

The semi-major axis is then $a = C/A$, the distance δ between the foci is

$$\delta = 2a (1 - A^2)^{1/2} \quad (127b)$$

and the foci are on the x-axis at $x = -B \pm \delta/2$. To assign a given point, we form its distances (R_1, R_2) from the two foci: if

$$2(a-1) < R_1 + R_2 < 2a$$

the point has IREG=1, and if

$$2R_E < R_1 + R_2 < 2(a+1)$$

it has IREG=2. If $R_1 + R_2$ is bigger still, the point's position relative to the bow shock should be tested.

4.8.2 The Bow Shock

Fairfield in 1971 approximated the shock position in AGSM by a hyperboloid (one rather close to a paraboloid)

$$F_2(\mathbf{r}) = R^2 + A x R + B x^2 + C R + D x + E = 0 \quad (128)$$

where

$$A = 0.0296 \quad B = -0.0381 \quad C = -1.28 \quad D = 45.644 \quad E = -652.1$$

The subsolar distance is close to $1.3 r_s$. As in the SSC code, this distance can be scaled so that when different values of (p/p_0) change r_s , the hyperboloid scales to a larger or smaller one of the same shape but still cuts the x-axis at $1.3 x_{ss}$. Such scaling occurs if we replace

$$R \rightarrow kR \quad x \rightarrow kx$$

The subsolar point of the hyperboloid is reached when $R=0$, i.e. when

$$B(kx)^2 + D(kx) + E = 0$$

$$kx = \frac{1}{2B} (-D + [D^2 - 4BE]^{1/2}) = x_0 \quad (129a)$$

Here x_0 is a constant derivable from the constants of (128). If the subsolar distance of the magnetopause is x_{ss} , the value of x for which (133a) is satisfied should be $1.3 r_s$, hence

$$k = x_0 / 1.3 r_s \quad (129b)$$

Equation (128) is then modified by multiplying (R^2, A, B) by k^2 , and (C, D) by k . If $F_2 > 0$, the point is in the solar wind, otherwise it is inside the bow shock.

4.8.3 The Equatorial Surface

If the Earth's dipole is perpendicular to the direction of the solar wind--as happens twice a day in two parts of the year, near equinox--then the magnetospheric field is expected to have north-south symmetry across the equatorial plane $z_{sm} = 0$.

At all other times the equatorial surface (which may be defined as the surface where B_p reverses sign, where $\rho^2 = x^2 + y^2$) is observed to be deformed. Near Earth it approximates the dipole's equatorial plane,

while in the fat tail its field lines tend to become aligned with the $\pm x_{sm}$ direction, defined by the solar wind.

Observations suggest that near midnight each the plasma sheet behaves as if attached to the equatorial plane of the dipole at a distance of about $R_H = 8 R_E$, so that it is displaced from the $z=0$ plane by $R_H \sin\psi$, up to about $4 R_E$. However, the magnetopause is observed to depart very little from north-south symmetry, even when ψ is large.

Since the northern and southern halves of the tail contain the same amounts of magnetic flux, one would then expand the “hinging” to expand one side of the tail and compress the other, reducing the magnetic field intensity B on the expanded side and increasing it on the compressed one. Plasma pressure considerations however require B in the northern and southern tail lobes, at any given distance, to be about equal. Hence the equator warps in a way that displaces it near the flanks in the **opposite** direction to its displacement near midnight: if at midnight the equator is displaced northward, its sections near the magnetopause move southward.

Empirical formulas for such displacements were derived by Fairfield, Gosling and others, but the one used here is due to Tsyganenko and is also used by the SSC. The use of that formula however needs modification, because it does not give the equator as defined by B_ρ , instead, it gives the center of a current distribution used as the source of the tail field in Tsyganenko’s model. Far from Earth, this is very close to the center of the displaced plasma sheet, but near Earth the fields of the dipole and ring current enforce their own symmetry, which tends to center on the dipole equator, whose shape is flat, not warped.

Because of that, the full Tsyganenko formula is only used tailwards of $x_{sd} = -8 R_E$ (x_{sd} is the x -coordinate in the solar dipole frame, with the z axis along the dipole and x_{sd} in the GSM $y=0$ plane). Sunward of $x_{sd} = 0$, the dipole equator is used, and for $0 > x_{sd} > -8$, the part of the formula expressing the y -dependent warping is linearly interpolated as a function of x_{sd} .

The shape of the equatorial surface is given by a function

$$z = z_s(x, y, \psi) \quad (130)$$

with ψ the tilt angle: z_s is the distance one must move north from $(x, y, 0)$ (or south, if $z_s < 0$) in order to reach the equatorial surface. Tsyganenko approximated

$$z_s(x, y, \psi) = z_{s1}(x, \psi) + z_{s2}(y, \psi) \quad (131a)$$

with

$$z_{s1}(x, \psi) = 0.5 \tan\psi \left[(u^2 - 2R_H x \cos\psi)^{1/2} - (u^2 + 2R_H x \cos\psi)^{1/2} \right] \quad (131b)$$

where

$$u^2 = x^2 + (R_H^2 + \Delta x^2) \cos^2\psi$$

and

$$z_{s2}(y, \psi) = G \sin\psi \frac{y^4}{y^4 + L^4} \quad (131c)$$

Here $R_H = 8 R_E$ is the hinging distance, and for small values of $|x|$, (135b) gives

$$z_{s1}(x, \psi) \rightarrow -\frac{x}{u} R_H \sin\psi \quad (132)$$

Other constants (all measured in R_E) are $\Delta x = 4$, $L = 10$, $G = 10$. By (131b), z_{s1} smoothly tends to near the dipole equator as x approaches zero, and is therefore retained in the range $0 > x > -8$. However, z_{s2} does not change to match the flat dipolar equator, and is therefore multiplied in that region by a (positive) factor $0 < -x_{sd}/8 < 1$.

4.9 Launch Windows

4.9.1 General Considerations

Since "Profile" satellites are meant to be small and cheap, they are not expected to carry any propulsion. The only control over their orbit is then an appropriate choice of launch conditions. If the launch is assumed to be from Cape Canaveral and towards the East, only a few adjustable parameters remain. Two parameters are obviously the **time of day** of the launch and the **day of the year** on which it takes place.

A third parameter is available if a 4-stage launcher is used, so that the first three stages place the "Profile" bus in a circular parking orbit and the 4th stage then injects it into its long ellipse. The **delay** between launch and injection then provides a third parameter determining the choice of orbit. As will be seen, the first and third parameters determine Ω and ω of the orbit; the orbital inclination i is fixed by the latitude of the launch, which is 28.5° .

Not considered here are possible shifts of the launch direction from east, which modify i and require rather small Δv . Also, the parking orbit will be assumed to begin at Cape Canaveral, latitude 28.5° and longitude -80.5° ; in an actual launch, a certain horizontal distance is covered by the rocket, and the parking orbit is entered further east. The injection by the 4th stage is similarly assumed to be instantaneous. It is assumed that all orbits obtained here are also feasible with acceleration distances taken into account, though the firing times may have to be shifted.

Before selecting launch parameters, one must decide on **criteria** for evaluating candidate orbits. Obviously, the **orbital lifetime** should be long, and perigee height should not drop into the atmosphere, but rather, rise higher. These considerations involve the perturbation of the Sun, Moon and the Earth's equatorial bulge, and will be dealt with in a later section, but it can be stated here that **date of launch** is the most useful variable here.

For a magnetospheric mission, **coverage of the plasma sheet** should be as extensive as possible, since that region is the sources of aurora, storms and other activities. Naively one may expect that an orbit whose plane is close to the ecliptic is best here. Unfortunately, orbits close to the ecliptic also spend relatively long times in the **Earth's shadow**, where electric power is not produced, the satellite cools down drastically and stored electricity must be used to keep batteries from freezing.

4.9.2 Determining ω and Ω

In each revolution of the Earth, the radius from the origin to Cape Canaveral describes a cone with half-opening angle $90^\circ - 28.5^\circ = 61.5^\circ$. Because the Earth's axis is inclined to the ecliptic by an angle $\epsilon \approx 23.5^\circ$, the angle between the radius to Cape Canaveral and its projection on the plane of the ecliptic varies each day between $28.5^\circ - \epsilon \approx 38^\circ$ and $28.5^\circ + \epsilon \approx 52^\circ$ (see figure).

The orbital plane of the satellite is tangential to the cone at the point of launch, and its inclination i_e to the plane of the ecliptic therefore also has the range

$$28.5^0 - \epsilon < i_e < 28.5^0 + \epsilon$$

The actual value of i_e will depend on the time of launch. Each day has one "reference time" t_r at which a launch gives the bus carrying the satellites its smallest possible i_e , about 5^0 . The orbit obtained by launching at that time and immediately following that with 4th stage firing will be termed the **reference orbit**.

Suppose the plane of the paper in the above figure includes two generating lines of the cone, specifically, the ones with smallest (5^0) and largest (52^0) values of i_e . Then the ecliptic x_e axis is perpendicular to the paper and is directed out of it.

The plane of the reference orbit, tangential to the cone along AO, is also perpendicular to it, and it follows that the x_e axis lies in the orbital plane. However, the x_e axis is the same as the celestial x axis, and therefore also lies in the celestial equator. This makes it the **line of nodes** of the reference orbit, so that this orbit has

$$\Omega = 0 \quad (133)$$

If the 4th stage fires at point A, and it is assumed that the final speed is acquired there instantaneously (again, an approximation), then point A will also be the **perigee** point of the orbit. Thus the angle between the line of nodes (which is also the x-axis) and the radius to perigee is 90^0 , providing another orbital element

$$\omega = 90^0 \quad (134)$$

Even though the reference orbit has the smallest possible inclination to the plane of the ecliptic, it does not provide very good coverage of the plasma sheet. The preceding figure gives the orientation of that orbit in (x_e, y_e, z_e) space, where the Sun appears to rotate in the course of the year around the (x_e, y_e) plane.

Perigee is at point A in the (y_e, z_e) plane, and apogee is in that plane too, on the other side. For apogee to be in the middle of the tail, the Sun must be on the same plane, i.e. at the winter solstice (see figure). Because the plasma sheet behaves as if it were hinged to the dipole equator (and here the difference between geographic and dipole equator is neglected), it will move away from the ecliptic, to the side of the ecliptic **opposite** the one of the orbit, greatly reducing tail coverage by the satellites.

Given a free choice of the time when the 4th stage ignites, this is readily remedied. If the firing is delayed until the satellite has moved 90^0 away from point A (a quarter-period for a circular orbit), it will be on the x-axis, placing both perigee and apogee on that axis--perigee with negative x, apogee with positive. Apogee is then in the tail during fall equinox, when plasma sheet deformation is at its smallest, giving very good tail coverage.

Alternatively, if firing is delayed until a 270^0 arc has been completed, apogee will be in the tail at the spring equinox. Of course, either delay can be increased by an arbitrary whole number of orbital periods.

The general orbit can thus be characterized by two numbers. One is the delay δ_1 (of either sign, in degrees or in hours, $1 \text{ hr} = 15^0$) of the launch time relative to that of the reference orbit. The other is the length of the "coasting arc" δ_2 (in degrees), spent in the parking orbit between launch and 4th stage ignition. In terms of orbital elements

$$\begin{aligned}\Omega &= \delta_1 \\ \omega &= 90^\circ + \delta_2\end{aligned}\quad (135)$$

4.9.3 Eclipses

All “Profile” satellites are expected to pass through the Earth’s shadow once per orbit. During an eclipse, solar cells provide no power and the satellite cools down. Scientific data-gathering will probably have to stop, but power is still needed for heating batteries to keep them from freezing, and also for maintaining essential functions, e.g. for the computer’s memory and clock. Eclipses near perigee are brief and will not be considered here, but distant ones pose a serious problem.

The previous section concluded that the best coverage of the plasma sheet is achieved by orbits with minimal inclination i_e to the ecliptic and with apogee on the x-axis ($\Omega=0$, $\omega = 0$ or 180°). Unfortunately, placing the apogee on the x axis means that once a year, near one of the equinoxes, it will be in the Earth’s shadow. Near apogee the satellites moves very slowly, and their eclipses there are quite long. Because of the smallness of i_e , before and after that equinox other distant parts of the orbit will also hit the shadow, causing additional long eclipses.

As long as we plan to cover the plasma sheet during equinox, this problem will persist, because at that time of the year, the Earth’s shadow is also cast right down the plasma sheet. Any practical orbit thus requires a certain compromise.

One way of obtaining a better understanding of distant eclipses is to express the direction of the vector $\hat{\xi}$, pointing towards perigee, in ecliptic coordinates (x_e, y_e, z_e). Using the transpose of the matrix **A** of eq. (79), we have here

$$\begin{pmatrix} \xi \\ \eta \\ \zeta \end{pmatrix} = \mathbf{A}^T \begin{pmatrix} x \\ y \\ z \end{pmatrix} \quad (81)$$

Let the top row of \mathbf{A}^T be (a_1, a_2, a_3). Then

$$\hat{\xi} = a_1 \hat{x} + a_2 \hat{y} + a_3 \hat{z} \quad (136)$$

and by eq. (79)

$$\begin{aligned}a_1 &= \cos\omega \cos\Omega - \cos i \sin\omega \sin\Omega \\ a_2 &= \cos\omega \sin\Omega + \cos i \sin\omega \cos\Omega \\ a_3 &= \sin i \sin\omega\end{aligned} \quad (137)$$

By (95)

$$\begin{pmatrix} x \\ y \\ z \end{pmatrix} = \mathbf{A}_3^T \begin{pmatrix} x_e \\ y_e \\ z_e \end{pmatrix} = \begin{pmatrix} 1 & 0 & 0 \\ 0 & \cos \varepsilon & -\sin \varepsilon \\ 0 & \sin \varepsilon & \cos \varepsilon \end{pmatrix} \begin{pmatrix} x_e \\ y_e \\ z_e \end{pmatrix} \quad (138)$$

where $\varepsilon = 23.45^\circ$ is the inclination of the Earth’s axis. Thus

$$x = x_e \quad y = y_e \cos \varepsilon - z_e \sin \varepsilon \quad z = y_e \sin \varepsilon + z_e \cos \varepsilon \quad (139)$$

Hence by (137)

$$\xi = a_1 x_e + (a_2 \cos \varepsilon + a_3 \sin \varepsilon) y_e + (-a_2 \sin \varepsilon + a_3 \cos \varepsilon) z_e \quad (140)$$

with a similar relation between unit vectors.

The orientation of $\hat{\xi}$ in space may then be expressed by the angles (χ_1, χ_2) defined in the figure. If $\hat{\xi}_e$ is the projection of $\hat{\xi}$ on the (x_e, y_e) plane, i.e. on the ecliptic, then χ_1 is the angle between $\hat{\xi}_e$ and \hat{x} while χ_2 is the angle between $\hat{\xi}_e$ and the \hat{z}_e direction. We have from the scalar product

$$\sin\chi_1 = \hat{\xi} \cdot \hat{z}_e = -a_2 \sin\epsilon + a_3 \cos\epsilon \quad (141)$$

Also, $\tan\chi_2$ is the ratio between the y_e and x_e components of $\hat{\xi}$, i.e.

$$\tan\chi_2 = \frac{a_2 \cos\epsilon + a_3 \sin\epsilon}{a_1} \quad (142)$$

The angle χ_2 indicates the time of the year when perigee is on the midnight meridian: for instance, if $\chi_2 = (0, 90^\circ, 180^\circ, 270^\circ)$, this happens on an equinox or solstice in (fall, winter, spring, summer). Since apogee is always on the *opposite* side of Earth from perigee, it follows that for the same four values of χ_2 , *apogee* is in the tail in (spring, summer, fall, winter).

More generally, let Ω_s be the angle between the direction of the Sun and the x (or x_e) direction. To calculate its approximate value, assume the spring equinox falls on day 80 of the year and the Sun's motion around the ecliptic is uniform. Then on day-of-the-year D

$$\Omega_s \approx (D - 80) \frac{360}{365}$$

Then as the figure makes clear, apogee is at midnight on the day when $\Omega_s = \chi_2$, i.e. for day

$$D = \left(\frac{365}{360} \right) \chi_2 + 80$$

(subtract 365 if the sum exceeds 365).

The angle χ_1 indicates the displacement of perigee (and hence also of apogee) from the plane of the ecliptic.

If χ_1 is small, apogee is close to the ecliptic, and the orbit may be vulnerable to long eclipses far from Earth. If then $\chi_2 = (0, 180^\circ)$ apogee is in the tail during equinox and plasma sheet coverage is good; if on the other hand $\chi_2 = (90^\circ, 270^\circ)$, apogee will tend to miss the midnight plasma sheet, because the warping effect is then at its greatest and the midnight plasma sheet, being hinged to the magnetic equator, is displaced from the plane of the ecliptic. If χ_1 is large, e.g. $\chi_1 > 45^\circ$, apogee will always miss the plasma sheet, no matter what the value of χ_2 may be.

4.9.4 Eclipses in Keplerian simulations

In the first round of simulations, described further below, 12 satellites of a simulated “Profile” mission were followed for a year, assuming strict Keplerian motion, and were examined once every hour. Each time note was taken, among other things, of whether the satellite was in the Earth’s shadow beyond $r = 2 R_E$ and if so, a tally was kept of the number of later checks which found it still eclipsed.

The Earth’s shadow was assumed to be a cylinder of radius $1 R_E$ with its axis along the Sun’s direction. That seemed a reasonable approximation, considering that at $r=20 R_E$ the penumbra--the region in which some of the Sun is obscured but not all of it--is only $0.2 R_E$ wide. One-time shadow passes were taken to be 1 hour long, those with two consecutive positions in the shadow 2 hours, and so on.

The orbit with greatest plasma sheet coverage ($\Omega = 0$, $\omega = 180^\circ$) and orbits close to it had conspicuous “shadow seasons” around the fall equinox, with eclipses lasting up to 7 hours at its peak. Relatively long eclipses also existed before and after the peak, their duration decreasing as one went away from the time of their peak. For other orbital conditions, less severe “shadow seasons” were noted, and at times two peaks were found, with various separations.

Eclipses are best studied in the frame of ecliptic coordinates (x_e, y_e, z_e) which, like the celestial frame (x, y, z), is also an inertial frame. Consequently one can calculate in it orbital elements, distinguishing them by subscript “e”. The three elements (a_e, e_e, l_e) are the same in both frames, but the remaining three (i_e, ω_e, Ω_e) are not and must be derived separately.

The derivation is quite similar to that of (i, ω, Ω), which started from the matrix **A** for which

$$\begin{pmatrix} x \\ y \\ z \end{pmatrix} = \mathbf{A} \cdot \begin{pmatrix} \xi \\ \eta \\ \zeta \end{pmatrix} \quad (78)$$

and whose terms could also be expressed by (i, ω, Ω). Using the factorization (87) of **A**, equations were obtained which allowed the three angles to be computed. Since by eq. (95)

$$\begin{pmatrix} x_e \\ y_e \\ z_e \end{pmatrix} = \begin{pmatrix} 1 & 0 & 0 \\ 0 & \cos \epsilon & -\sin \epsilon \\ 0 & \sin \epsilon & \cos \epsilon \end{pmatrix} \begin{pmatrix} x \\ y \\ z \end{pmatrix} = \mathbf{A}_3 \cdot \begin{pmatrix} x \\ y \\ z \end{pmatrix} \quad (95b)$$

we get

$$\begin{pmatrix} x \\ y \\ z \end{pmatrix} = \mathbf{a} \cdot \begin{pmatrix} \xi \\ \eta \\ \zeta \end{pmatrix} \quad (143a)$$

where

$$\mathbf{a} = \mathbf{A}_3 \mathbf{A} \quad (143b)$$

The whole procedure can then be repeated, but with a_{ij} replacing A_{ij} everywhere.

If i_e is **not** small, eclipses can occur only near two points on the orbit, the two points at which it intersects the ecliptic, located on the line of nodes (top Figure).

One can then divide the orbit into two unequal parts by a line through the origin, perpendicular to the long axis of the orbit (bottom Figure): the small “near” part centered on perigee, and

the much larger “distant” part centered on apogee. The line of nodes passes through the origin too and it therefore has one orbital intersection in each part. Eclipses that occur in the “near” part, however, are not counted; therefore only distant ones contribute to a “shadow season” and only one such season per orbit is expected.

Calculating the time of that season is similar to deriving the effect of χ_2 : the Earth’s shadow is projected along the line of nodes twice a year, when Ω_s equals either Ω_e or $\Omega_e + 180^\circ$. The first of these is when the shadow is directed towards the distant crossing. Thus the “shadow season” is expected to peak when

$$\Omega_s = \Omega_e \quad (144)$$

The shadow season is expected to become shorter when i_e increases, because steeply inclined orbits quickly move away from the shadow cylinder. Eclipses are longest when $\omega_e = 0, 180^\circ$ and shadows occur at apogee, and shortest when $\omega_e = 90^\circ, 270^\circ$ at which time they occur so close to Earth that they might even miss being counted at all.

For orbits with **small** inclination i_e the situation is somewhat different, because eclipses can now occur even some distance from the line of nodes; in the limiting case of $i_e = 0$, they can occur in *any* part of the orbit. If ω_e is near 0° or 180° , eclipses occur near apogee and one can expect a long season around them. If on the other hand ω is near 90° or 270° , apogee will be relatively far from the ecliptic, but eclipses can extend for some distance along the line of nodes on both flanks of the orbit: in that case two moderate shadow seasons are expected.

In summary, it seems that eclipses are best avoided if i_e is moderately large, e.g. 10° . However, perturbations due to the Moon etc. will cause i_e to change with time, and that change must also be simulated, throughout the mission. Ultimately it may well turn out that the ability to survive long eclipses (e.g. up to 3 hours or even more) will be one of the requirements of a protracted mission.

4.10 Simulation of Magnetospheric Coverage

4.10.1 The ORB5 code

To provide information on the expected coverage and to test the preceding ideas, a Fortran code ORB5 was produced. Its **inputs** are a launch date and the launch parameters (delay and coasting arc) which determine the angles (δ_1, δ_2) of (135). Its **outputs** are statistics of region occupancy, eclipses and other features over the course of one year, or more accurately, over a time span of 52 weeks (364 days).

The code employs a number of subroutines: ORBEL produces orbital elements corresponding to given values of $(\mathbf{r}_0, \mathbf{v}_0)$, while ORBPT inverts the process and gives \mathbf{r} for any given time t (\mathbf{v} can also be extracted, but was not included because it is rarely needed). TRANS4 (a package of several small codes) calculated rotation matrices between various frames at a given time t , MSREG assigned a region in the magnetosphere to a given (x, y, z, t) and NSHEET found the value of z in the neutral sheet (or more generally, on the equatorial surface) corresponding to given (x, y, t) . The usual altitude of perigee was $1.1 R_E$.

The orbit with minimal i_e has the property that its perigee is in the yz plane, while the sidereal time at a given point is the angle between its meridian and the xz plane. We now use a formula by Meeus [1991, eq. 11.3] for the sidereal time θ_0 at Greenwich at UT=0 on a given Julian date (i.e. for a Julian time that ends in 0.5). Launch from Cape Canaveral for a satellite attaining the orbit with smallest i_e must be at the UT corresponding to $\theta_0 = 170.5^\circ$, because Greenwich lies 80.5° east of Canaveral and the meridian of Cape Canaveral should be on the yz plane which is 90° east of the xz plane. Introducing (δ_1, δ_2) of (135), a delay of the launch by $\delta_1/15$ hours shifts Ω by δ_1 degrees, while allowing the satellite to coast in its parking orbit over an angle $\delta_2 + 90^\circ$ shifts ω by the same amount. Both the delay and the "coasting arc" are entered from the keyboard.

The calculation is quite fast, because the orbit is fixed in inertial space and the orbital period is an integral number of hours, 48 in this case. Thus whenever the position of the multiprobes is examined, any of them can only occupy one of 48 set positions. As time advances hour by hour, it is only necessary to permute the satellite positions around the orbit and they never have to be recalculated.

However, the positions of the multiprobes relative to the magnetosphere--even relative to the averaged magnetosphere--varies constantly, as the angle between the major axis of the orbit and the solar wind undergoes its annual 360° rotation, while the tail sheet warps and the dipole axis turns with the Earth's own diurnal rotation. Thus the transformation matrices to the GMS frame must be recalculated every hour. For every one of those hours, the program collects information about the frequency at which various types of coverage occur.

Obviously, at each position and for each satellite, subroutine MSREG must assign the satellite to one of 10 regions of the magnetosphere (though the latitude is never high enough for region 9); to assign tail regions, MSRG in its turn calls NSHEET.

Since it was assumed that no data are collected during eclipses, any satellite in the Earth's shadow is not included in any other statistics. In the simulation, each satellite, at any time, was assigned a status number LS, telling how many hours it had spent in eclipse: whenever the satellite was found to be eclipsed, its LS is increased by 1. If the satellite was *not* eclipsed, its current value of LS was examined, and if that value was not zero, the tally of shadows of length LS for that particular week was increased by 1, and LS was reset to zero.

Statistics were furthermore collected for any hour (out of 168 hours per week) on the number of satellites simultaneously in the plasma sheet, in the range $r_{\min} < r < r_{\max}$, where radial limits were specified from the keyboard. Finally, the number of satellites which at any hour were within $\pm 1 R_E$ of the magnetopause was also recorded.

Such statistics were compiled week by week, as well as for four "seasons" of 13 weeks each and for the entire "year" of 364 days. The sample orbits listed in Tables were obtained for the "reference orbit" and for a "good" orbit, both assuming launch on 7.25.1997. The distribution of eclipses of various lengths occurring for the "reference orbit" outside $r=2 R_E$ is also given here, with superimposed eclipses of the "good" orbit in parentheses.

4.10.2 The ORB6 code

While the preceding simulation provides a fair view of the coverage of the magnetosphere by "Profile," the mission actually planned differs in one important way, namely, it would include two groups of 6 satellites, with slightly different orbits. A simulation code ORB6 was therefore developed from the preceding one, tracking two groups of satellites, one with period 48 hours and one with a period 46 hours.

All the preceding statistics were again collected, but weekly statistics were also tallied for the following additional "constellations":

- (1) At times the satellites covered the plasma sheet for $r_{\min} < r < r_{\max}$ on both legs of the orbit, outbound from Earth and inbound, giving a somewhat 2-dimensional coverage. ORB6 then recorded the number of weekly hours (out of a total of 168) during which the two sides of the plasma sheet (neutral sheet $\pm 3 R_E$) were covered by (2,2), (2,3+) or (3+,3+) satellites.
- (2) The two-group mission makes possible "superclusters" of 8, 9, 10 or 11+ satellites, all in the region $r > 19 R_E$, near apogee. The number of weekly hours for each "supercluster" size was recorded, and as expected, it peaked in a 7-week cycle, corresponding to the time needed for one group to overtake the other.

The number of superclusters in the plasma sheet (neutral sheet $\pm 3 R_E$) was also recorded: these tended to occur in two of the specific "seasons", 7 weeks apart.

- (3) ORB6 also tallied the number of hours each week when at least 2 satellites were simultaneously in each of 4 regions--solar wind, magnetosheath (far from the magnetopause), $\pm 1 R_E$ of the magnetopause and the inner magnetosphere. Tally was also kept of the hours when the requirement for the solar wind was not satisfied (e.g. when the satellites may have been too far from the Sun-Earth line to reach the bow shock) but with (2+, 2+, 3+) satellites in the other three regions.

Some results are given in table Actual orbits, of course, gradually change their elements due to external perturbations, but if such changes are known, similar codes can also be written for them.

4.11 Orbital perturbations

4.11.1 The Disturbing Acceleration a

Let subscripts (1,2,3,4) refer to (Earth, satellite, Moon, Sun), and let G be the gravitational constant. Then equations (8) can be generalized to

$$\frac{d^2 \mathbf{r}_1}{dt^2} = G \frac{m_2}{r_{12}^3} (\mathbf{r}_2 - \mathbf{r}_1) + G \frac{m_3}{r_{13}^3} (\mathbf{r}_3 - \mathbf{r}_1) + G \frac{m_4}{r_{14}^3} (\mathbf{r}_4 - \mathbf{r}_1) \quad (145a)$$

$$\frac{d^2 \mathbf{r}_2}{dt^2} = G \frac{m_1}{r_{21}^3} (\mathbf{r}_1 - \mathbf{r}_2) + G \frac{m_3}{r_{23}^3} (\mathbf{r}_3 - \mathbf{r}_2) + G \frac{m_4}{r_{24}^3} (\mathbf{r}_4 - \mathbf{r}_2) \quad (145b)$$

The vectors \mathbf{r}_i are in inertial space, and since all four bodies move, none can provide a fixed point to which they can be referred. However, one can deal exclusively in **differences**. Let

$$\mathbf{r} = \mathbf{r}_2 - \mathbf{r}_1 \quad \boldsymbol{\rho}_3 = \mathbf{r}_3 - \mathbf{r}_1 \quad \mathbf{d}_3 = \mathbf{r}_2 - \mathbf{r}_3 = \mathbf{r} - \boldsymbol{\rho}_3 \quad (146a)$$

$$\boldsymbol{\rho}_4 = \mathbf{r}_4 - \mathbf{r}_1 \quad \mathbf{d}_4 = \mathbf{r}_2 - \mathbf{r}_4 = \mathbf{r} - \boldsymbol{\rho}_4 \quad (146b)$$

(\mathbf{r} is vector Earth to satellite
 $\boldsymbol{\rho}_i$ is vector from Earth to i th body,
 \mathbf{d}_i vector from i th body to satellite)

Subtracting (145a) from (145b), with $\mu = G(m_1 + m_2) \approx Gm_1 = g R_E^2$

$$\frac{d^2 \mathbf{r}}{dt^2} + \frac{\mu}{r^3} \mathbf{r} = -\mu \frac{m_3}{m_1} \left[\frac{1}{d_3^3} \mathbf{d}_3 + \frac{1}{\rho_3^3} \boldsymbol{\rho}_3 \right] - \mu \frac{m_4}{m_1} \left[\frac{1}{d_4^3} \mathbf{d}_4 + \frac{1}{\rho_4^3} \boldsymbol{\rho}_4 \right]$$

$$= -\mu \frac{m_3}{m_1} \left[\frac{1}{d_3^3} (\mathbf{r} - \mathbf{p}_3) + \frac{1}{\rho_3^3} \mathbf{p}_3 \right] - \mu \frac{m_4}{m_1} \left[\frac{1}{d_4^3} (\mathbf{r} - \mathbf{p}_4) + \frac{1}{\rho_4^3} \mathbf{p}_4 \right] \quad (147)$$

The perturbation caused by the moon needs no further attention, but that of the Sun does, because it contains two large terms of opposite signs, almost equal. We have

$$\begin{aligned} d_4^2 &= (\mathbf{r} - \mathbf{p}_4)^2 \approx \rho_4^2 - (2\mathbf{r} \cdot \mathbf{p}_4 - r^2) \\ &= \rho_4^2 (1 - [2\mathbf{r} \cdot \mathbf{p}_4 - r^2] / \rho_4^2) = \rho_4^2 (1 - \text{SCP}) \end{aligned} \quad (148a)$$

where the scalar product term SCP is $\ll 1$. Then

$$\begin{aligned} d_4^{-3} &\approx \rho_4^{-3} (1 - \text{SCP})^{-3/2} \approx \rho_4^{-3} \left[1 + \frac{3}{2} \text{SCP} + \left(\frac{-3}{2} \frac{-5}{2} \frac{1}{2} \right) \text{SCP}^2 \right] = \\ &= \rho_4^{-3} (1 + \text{SCP} * (1.5 + 1.875 * \text{SCP})) \\ &= \rho_4^{-3} (1 + \text{SCPA}) \end{aligned} \quad (148b)$$

The last brackets in **(147)** thus become

$$\begin{aligned} \left[\frac{1}{d_4^3} (\mathbf{r} - \mathbf{p}_4) + \frac{1}{\rho_4^3} \mathbf{p}_4 \right] &\approx \frac{1}{\rho_4^3} \left[(\mathbf{r} - \mathbf{p}_4)(1 + \text{SCPA}) + \mathbf{p}_4 \right] = \\ &\approx \frac{1}{\rho_4^3} \left[\mathbf{r} (1 + \text{SCPA}) - \mathbf{p}_4 \text{SCPA} \right] \end{aligned} \quad (149)$$

Hence the perturbing acceleration \mathbf{a} , on the right side of eq, **(13)**, is very nearly

$$\mathbf{a} = -\mu \frac{m_3}{m_1} \left[\frac{1}{d_3^3} (\mathbf{r} - \mathbf{p}_3) + \frac{1}{\rho_3^3} \mathbf{p}_3 \right] - \mu \frac{m_4}{m_1} \frac{1}{\rho_4^3} \left[\mathbf{r} (1 + \text{SCPA}) - \mathbf{p}_4 \text{SCPA} \right] \quad (150)$$

where \mathbf{p}_3 is the vector from Earth to the moon, \mathbf{p}_4 is from Earth to the Sun, and d_3 is the magnitude of $(\mathbf{r} - \mathbf{p}_3)$. Approximation **(149)** may also be used for the moon, but seems too inaccurate there. We used the values

$$\begin{aligned} \mu (m_{\text{moon}}/m_{\text{earth}}) &= 4.8964796 \cdot 10^{12} \\ (m_{\text{sun}}/m_{\text{moon}}) &= 2.707309 \cdot 10^7 \end{aligned}$$

4.11.2 Orders of Magnitude

The distance to the moon is about 1/400 AU. The mass of the moon is 1/80 that of the Earth, which is in turn $\approx 10^6$ times smaller than the Sun's. We assume \mathbf{r} is about 1/3 of d_3 .

Then the order of magnitude of the solar terms compared to the lunar ones is

$$80 \cdot 10^6 \cdot (1/3) \cdot (1/400)^3 = 80/192 \approx 0.4$$

Thus the terms are comparable. The moon's attraction on the satellite is largest when the satellite is at apogee and the moon happens to be in the same direction. "Profile" apogee is about 1/3 the moon's mean distance, and the distance to the moon is then twice that to Earth, the moon's mass is 1/80, making the attraction

$$(1/80) \cdot (1/4) = 1/320$$

that of Earth.

4.11.3 The Non-Spherical Earth

The gravity field of a nonspherical Earth is usually expressed by assuming it is given by a scalar potential V

$$\mathbf{a} = -\nabla V \quad (151a)$$

and that V is given by an expansion in spherical harmonics. The potential V is assumed to be given, and has been obtained directly from the orbital variations of satellites in low Earth orbit. The biggest effects are the ones due to the Earth's oblateness, especially the second harmonic term J_2 .

We neglect the asymmetric terms, which are small and rather troublesome--expressed in geographic coordinates, they must be transformed to the celestial frame, a time-dependent transformation. The axisymmetrical terms need not be transformed, since (r, θ) are the same in geographic and celestial coordinates, and they include the dominant J_2 term. Thus

$$V = \frac{Gm}{r} \left[1 - \sum_2 J_k \left(\frac{R_{eq}}{r} \right)^k P_k(\cos\theta) \right] \quad (151b)$$

where the Earth's equatorial radius is $R_{eq} = 6378.39$ km. We have

$$P_0 = 1 \quad P_1 = \cos\theta \quad P_2 = \frac{1}{2}(3\cos^2\theta - 1) \quad P_3 = \frac{1}{2}(5\cos^3\theta - 3\cos\theta) \quad (152)$$

and recursively for any k ($v = \cos\theta$)

$$k P_k(v) - (2k-1) v P_{k-1}(v) + (k-1) P_{k-2}(v) = 0 \quad (153a)$$

From this

$$k P'_k - (2k-1)[v P'_{k-1} + P_{k-1}] + (k-1) P'_{k-2} = 0 \quad (153b)$$

which allows the derivative P'_k to be derived recursively as well, starting from $P'_0 = 0$, $P'_1 = 1$.

We derive ∇V in mixed coordinates, in terms of spherical r and cylindrical z (ultimately, we aim at cartesian components). For a satellite's motion, $Gm = \mu$ and we have

$$\cos\theta = z/r \quad (154)$$

hence for unit mass

$$V = \mu/r - \mu \sum_2 J_k R_{eq}^k r^{-(k+1)} P_k(z/r) \quad (155)$$

$$\nabla V = -\frac{\mu}{r^3} \mathbf{r} - \mu \sum_2 J_k R_{eq}^k \left[\left(-(k+1)r^{-(k+3)} P_k - z r^{-(k+4)} P'_k \right) \mathbf{r} + r^{-(k+2)} P'_k \hat{\mathbf{z}} \right] \quad (156)$$

However, an identity exists

$$P'_{k+1} - v P'_k = (k+1) P_k \quad (157)$$

so

$$\nabla V = -\frac{\mu}{r^3} \mathbf{r} + \mu \sum_2 J_k R_{eq}^k r^{-(k+3)} \left[P'_{k+1}(z/r) \mathbf{r} - r P'_k(z/r) \hat{\mathbf{z}} \right] \quad (158)$$

The acceleration due to oblateness is then

$$\mathbf{a} = \frac{\mu}{r^3} \sum_2 J_k (R_{eq}/r)^k \left[P'_{k+1}(z/r) \mathbf{r} - r P'_k(z/r) \hat{\mathbf{z}} \right] \quad (159)$$

Accepted values of the coefficients, in units of 10^{-6} , are [reference...]

$$J_2 = 1082.63 \quad J_3 = -2.54 \quad J_4 = -1.62 \quad J_5 = -0.23 \quad J_6 = -0.55 \quad (160)$$

4.11.4 Low Precision Formulas for Postions of Sun and Moon

The Astronomical Almanac gives "low precision formulas" for the location of the Sun(p. C-24) and the Moon (p. D-46). Meeus [1991] has corresponding formulas: the one for the Sun is similar, but the one for the moon however is much longer and presumably more accurate, Since we use these bodies only to derive small perturbing terms, the formulas of the almanac were deemed sufficient.

Sun

On Julian date JF, let

$$n = \text{JD} - 2\,451\,545.0 \quad (161)$$

This is equivalent to T in the formulas of Meeus, except that n is in Julian days whereas T is in Julian centuries ($T = n/36525$).

Then the *mean longitude* of the Sun, "corrected for aberration" (which may explain the difference between the leading terms below)

$$L = 280.461 + 0.985\,6474\,n \quad (162a)$$

whereas Meeus gives

$$L = 280.46645 + 36000.76983\,T + 0.0003032\,T^2 \quad (162b)$$

The *mean anomaly* (of the Earth) in degrees is

$$g = 357.528 + 0.9856003\,n \quad (163a)$$

whereas Meeus denotes it by M and uses

$$M = 357.5290 + 35999.05030\,T - 0.000\,1559\,T^2 - 0.000\,000\,48\,T^3 \quad (163b)$$

Ecliptic longitude, in degrees

$$\lambda = L + 1.915 \sin g + 0.020 \sin 2g \quad (164a)$$

while Meeus gives on top of p. 152 as "*true longitude*"

$$\begin{aligned} \Theta = L &+ (1.914600 - 0.004\,817\,T - 0.000\,014\,T^2) \sin M \\ &+ (0.019\,993 - 0.000\,101\,T) \sin 2M + 0.000\,290 \sin 3M \end{aligned} \quad (164b)$$

The ecliptic latitude of the Sun by definition is zero, so the above gives the Sun's position on the celestial sphere.

Obliquity of the ecliptic, the angle between the Earth's axis and the z_e direction perpendicular to the ecliptic

$$\epsilon = 23.439 - 0.000\,0004\,n \quad (165)$$

(Meeus has an equivalent formula but in degrees, minutes and seconds, with terms to order T^3)

Distance R to the Sun, in astronomical units (AU)

$$R = 1.000\,14 - 0.016\,71 \cos g - 0.000\,14 \cos 2g \quad (166)$$

Meeus gives

$$R = 1.000\,01018 (1 - e^2)/1 + e \cos v$$

where v is the true anomaly $v = M + (O - L)$. To convert R to meters it is multiplied by $1 \text{ AU} = 1.49599 \cdot 10^{11}$ meters. The ecliptic coordinates of the Sun are then

$$(x_e, y_e, z_e) = (R \cos \lambda, R \sin \lambda, 0) \quad (167)$$

and the Sun's celestial coordinates

$$(x, y, z) = (x_e, y_e \cos \epsilon, y_e \sin \epsilon) = (R \cos \lambda, R \sin \lambda \cos \epsilon, R \sin \lambda \sin \epsilon) \quad (168)$$

The declination δ is the angle from the celestial equator: thus $(90^\circ - \delta)$ is the angle to the celestial z -axis, and its cosine is $(\hat{\mathbf{R}} \cdot \hat{\mathbf{z}})$. It follows that

$$\sin \delta = (\hat{\mathbf{R}} \cdot \hat{\mathbf{z}}) = \sin \lambda \sin \epsilon \quad (169)$$

Right ascension α satisfies $\tan \alpha = y_e/x_e$, hence

$$\tan \alpha = \frac{\cos \epsilon \sin \lambda}{\cos \lambda} = \cos \epsilon \tan \lambda \quad (170)$$

Moon

The position of the moon involves long, empirical formulas. The low precision formulas have 40 terms and are accurate to 0.3° in ecliptic longitude λ , 0.2° in ecliptic latitude β , $0.2 R_E$ in distance r . More accurate but much more complex formulas are given by Meeus and contain around 200 terms.

The almanac formulas use the same parameter T as Meeus:

$$T = \frac{\text{JD} - 2\,451\,545.0}{36525} \quad (90)$$

and defines a set of angles, named here arbitrarily and measured in degrees, as follows:

A0 = 218.32 + 481 267.883 T	A2 = 259.2 - 413 335.38 T
A1 = 134.9 + 477 198.85 T	A4 = 269.9 + 954 397.70 T
A3 = 235.7 + 890 534.23 T	A6 = 186.6 + 966 404.05 T
A5 = 357.5 + 35 999.05 T	
B1 = 93.3 + 483 202.03 T	B2 = 228.2 + 960 400.87 T
B3 = 318.3 + 6 003.18 T	B4 = 217.6 - 407 332.20 T
P1 = A1	P2 = A2
P3 = A3	P4 = A4

Then

$$\lambda = A0 + 6.29 \sin A1 - 1.27 \sin A2 + 0.66 \sin A3 + 0.21 \sin A4 - 0.19 \sin A5 - 0.11 \sin A6$$

$$\beta = 5.13 \sin B1 + 0.28 \sin B2 - 0.28 \sin B3 - 0.17 \sin B4$$

These give the ecliptic coordinates of the moon. to obtain the distance r , one first derives

$$\pi = 0.9508 + 0.0518 \cos P1 + 0.0095 \cos P2 + 0.0078 \cos P3 + 0.0028 \cos P4$$

and then

$$r = 1/\sin \pi$$

The three geocentric direction cosines $(l, m, n) = (c_1, c_2, c_3)$, i.e. the scalar products $\mathbf{r} \cdot \hat{\xi}$, $\mathbf{r} \cdot \hat{\eta}$ and $\mathbf{r} \cdot \hat{\zeta}$, are

$$\begin{aligned} c_1 &= \cos\beta \cos\lambda \\ c_2 &= 0.9175 \cos\beta \sin\lambda - 0.3978 \sin\beta \\ c_3 &= 0.3978 \cos\beta \sin\lambda + 0.9175 \sin\beta \end{aligned}$$

The celestial coordinates of the moon then are

$$x = c_1 r \quad y = c_2 r \quad z = c_3 r$$

4.11.5 Interpolating the positions of the Sun and Moon

The calculation of the Moon's position requires 16 trigonometric functions, that of the Sun's position 6. To calculate them at each step (and with Runge-Kutta integration, several times in each step) requires appreciable computer time. The calculation can be accelerated by the simple strategy of calculating positions ahead of time at a number (e.g. 100) of equally spaced values of the time t , and then interpolate linearly for any value of t that is given. That is especially important for the Moon, whose position takes longer to calculate and changes more rapidly than that of the Sun.

A subroutine FILLSUN was coded for this purpose. Given a value Δt , it derives at the beginning of the calculation an array of 101 positions of the Sun and Moon, corresponding to elapsed times of 0, Δt , ..., $100\Delta t$. After that, it performs two tasks. First, given time T , it interpolates between appropriate values of time and obtains the position of the Sun and Moon. And second, if T is within the top 10% of the array's range, it rennumbers its array, moves its last 11 values to the head of its new list, then derives 90 more positions so that a new array of 101 points is available, overlapping the old one in 10% of its length.

All lunar distances prepared for interpolation are multiplied by a factor FCT slightly larger than unity. The reason is that if we interpolate linearly between actual positions of the Moon, for all purposes and intents we are replacing the near-circular lunar orbit by a polygon enclosed inside it. In an enclosed polygon, the Moon-Earth distance is always *smaller* than the actual distance, leading to a systematic error. To avoid such a bias, the dimensions of the polygon are increased by a factor FCT, in such a way that the *area* enclosed by it approximately equals the area enclosed by the orbit. Interpolated points then may be outside the orbit or inside it, but on the average their distance will be close to the actual average distance.

Consider the orbital segment between two points A and B. Instead of interpolating along a chord AB, we extend the radial distances of A and B by a factor FCT, which moves them to points A' and B', between which the actual interpolation is made. The factor is defined by the requirement that the area of the triangle A'OB' is the same as that of the circular segment AOB. The area of the segment is

$$A_1 = r^2 \theta$$

and of A'OB'

$$A_2 = 2 (FCT)^2 r^2 \sin(\theta/2)$$

Since $A_1 = A_2$

$$FCT = \left(\frac{\theta}{2 \sin(\theta/2)} \right)^{1/2} \quad (161a)$$

Expanding

$$2 \sin(\theta/2) \approx \theta - \theta^3/24$$

$$\text{FCT} \approx (1 - \theta^2/24)^{-1/2} \approx 1 + \theta^2/48 \quad (161b)$$

Say the moon's orbit is divided into 60 segments: then $\theta = \pi/30$, $\theta^2/48 = 0.0002285$ and $\text{FCT} = 1.0002285$. With the same time interval, θ for the Sun is smaller by a factor 12, making the term added to unity 144 times smaller or 0.00000158: for now it will be neglected when dealing with the Sun.

4.12 Encke's Method

Encke's method is a straightforward perturbation calculation, i.e. we assume the motion is close to a Kepler ellipse and try to derive the difference. Let

$$\frac{d^2 \mathbf{r}}{dt^2} + \frac{\mu}{r^3} \mathbf{r} = \mathbf{a} \quad (162)$$

Given at $t=t_0$ initial parameters $\mathbf{r}_0 = \mathbf{r}(t_0)$, $\mathbf{v}_0 = \mathbf{v}(t_0)$, one can construct an unperturbed ("osculating") Kepler motion with those initial values

$$\frac{d^2 \mathbf{r}_{os}}{dt^2} + \frac{\mu}{r_{os}^3} \mathbf{r}_{os} = 0 \quad (163)$$

Positions and velocities on the osculating orbit at time t will be denoted $[\mathbf{r}_{os}(t), \mathbf{v}_{os}(t)]$. Let time advance to $t = t_0 + \Delta t$. Expanding the actual motion

$$\mathbf{r}(t) = \mathbf{r}(t_0) + \mathbf{v}_0(t_0) \Delta t + \frac{1}{2} \frac{d^2 \mathbf{r}}{dt^2}(t_0) \Delta t^2 + \dots \quad (164a)$$

while along the osculating ellipse

$$\mathbf{r}_{os}(t) = \mathbf{r}_{os}(t_0) + \frac{d\mathbf{r}_{os}}{dt}(t_0) \Delta t + \frac{1}{2} \frac{d^2 \mathbf{r}_{os}}{dt^2}(t_0) \Delta t^2 + \dots \quad (164b)$$

Subtract (164b) from (164a) and let

$$\boldsymbol{\delta}(t) = \mathbf{r}(t) - \mathbf{r}_{os}(t) \quad (165)$$

Since the two orbits share initial conditions, the two first right-hand terms are the same in (164a) and (164b). Subtracting, by (1) and (2)

$$\boldsymbol{\delta}(t) = \frac{1}{2} \left[\frac{d^2 \mathbf{r}}{dt^2}(t_0) - \frac{d^2 \mathbf{r}_{os}}{dt^2}(t_0) \right] \Delta t^2 = \frac{1}{2} \mathbf{a}(t_0) \Delta t^2 = \frac{1}{2} \frac{d^2 \boldsymbol{\delta}}{dt^2}(t_0) \Delta t^2 \quad (166)$$

Encke's method is to derive the time variation of $\boldsymbol{\delta}$, assuming that the motion itself follows the osculating orbit, along which the perturbing terms are derived. Inaccuracy enters because the values of \mathbf{a} used are for locations slightly off the particle's actual position, and similarly for other quantities which enter $\boldsymbol{\delta}$; but because all these errors occur in small quantities, the error is of a higher order.

If δ/r becomes too big (> 0.01 , one book suggests), the motion must be "rectified." Using $\boldsymbol{\delta}$ at the given point, we obtain (\mathbf{r}, \mathbf{v}) there, assume them to be the starting conditions of a new osculating orbit, and start again with a blank slate, i.e. with $\boldsymbol{\delta} = 0$.

Subtract (2) from (1) at some arbitrary later time

$$\begin{aligned}
 \frac{d^2\delta}{dt^2} &= \frac{\mu}{r_{os}^3} \mathbf{r}_{os} - \frac{\mu}{r^3} \mathbf{r} + \mathbf{a} \\
 &= \frac{\mu}{r_{os}^3} \left[\mathbf{r}_{os} - \frac{r_{os}^3}{r^3} \mathbf{r} \right] + \mathbf{a} \\
 &= \frac{\mu}{r_{os}^3} \left[\left(1 - \frac{r_{os}^3}{r^3}\right) \mathbf{r} - \delta \right] + \mathbf{a} \quad (167)
 \end{aligned}$$

This is an ordinary differential equation (ODE), or rather a set of ODEs, determining δ . It also contains $\mathbf{r}_{os}(t)$, a known function, and $\mathbf{r}(t)$, not known but expressible as $\mathbf{r} = \delta + \mathbf{r}_{os}$. One would have thought that we need eliminate \mathbf{r} , but the textbook I used [Battin, 1968] actually eliminates \mathbf{r}_{os} :

$$\begin{aligned}
 \mathbf{r}_{os} &= \mathbf{r} - \delta \\
 r_{os}^2 &= r^2 + \delta \cdot (\delta - 2\mathbf{r}) \\
 r_{os}^2/r^2 &= 1 + \delta \cdot (\delta - 2\mathbf{r})/r^2 = 1 + q \\
 r_{os}^3/r^3 &= (1 + q)^{3/2} \quad (168)
 \end{aligned}$$

and from this

$$1 - r_{os}^3/r^3 = 1 - (1 + q)^{3/2} = -f(q) \quad (169)$$

If q is small (as it should be, since it's of the order of δ), then $f(q)$ is also small, since it is the difference of two nearly identical terms. Multiplying by a suitable factor

$$f(q) [(1+q)^{3/2} + 1] = (1+q)^3 - 1 = 3q + 3q^2 + q^3 = q(3 + 3q + q^2)$$

hence

$$f(q) = q \frac{3+3q+q^2}{1+(1+q)^{3/2}} \quad (170)$$

which is clearly of order q , a function of q which need only be calculated once for all. Equation (167) now becomes

$$\frac{d^2\delta}{dt^2} = \frac{\mu}{r_{os}^3} (f(q)\mathbf{r} + \delta) + \mathbf{a} \quad (171)$$

If a new variable is defined $\mathbf{u} = d\delta/dt$, this breaks up into six equations (or two vectorial ones) of first order

$$\frac{d\delta}{dt} = \mathbf{u} \quad (172a)$$

$$\frac{d\mathbf{u}}{dt} = -\frac{\mu}{r_{os}^3} (f(q)\mathbf{r} + \delta) + \mathbf{a} \quad (172b)$$

The independent variable is time t , and \mathbf{r}_{os} depends on it. Let us follow the osculating orbit. Then $\mathbf{r}_{os}(t)$ is known, and we have a choice: either assume $\mathbf{r} \approx \mathbf{r}_{os}$, or else substitute $\mathbf{r} = \mathbf{r}_{os} + \delta$; to lowest order in δ , both give the same equation, but the second approach also retains some second order terms and will therefore be the one used here. Then

$$q = \frac{\delta \cdot (\delta - 2\mathbf{r})}{r^2} = -\frac{\delta \cdot (2\mathbf{r}_{os} + \delta)}{(\mathbf{r}_{os} + \delta)^2} = \frac{(2\mathbf{r}_{os} \cdot \delta) + \delta^2}{r_{os}^2 + (2\mathbf{r}_{os} \cdot \delta) + \delta^2} \quad (173)$$

and (172) becomes

$$\frac{d\delta}{dt} = \mathbf{u} \quad (174a)$$

$$\frac{d\mathbf{u}}{dt} = -\frac{\mu}{r_{os}^3} [\mathbf{f}(q)\mathbf{r}_{os} + (1+\mathbf{f}(q))\delta] + \mathbf{a} \quad (174b)$$

4.13 Runge-Kutta Integration

The methods used in integrating (174) were all taken from chapter 16 in *Numerical Recipes* [Press et al., 1992], a book which combines uncommonly lucid explanations with practical implementation codes. At first various adaptations of the tried-and-tested Runge-Kutta method were used, and were tested by checking the long-term behavior of the semimajor axis a , which is not supposed to vary. Since the semimajor axis is a function of the energy, the constancy of a can be interpreted as the conservation of energy when all time-dependent perturbations depend on periodically varying parameters. However, it can also be shown formally.

Runge-Kutta failed that test--not badly, but still, it failed (a similar problem was noted by Mullins and Evans [1996]). Then the method of Bulirsch and Stoer was tried, and it worked well. Had it failed,, a third approach, predictor-corrector schemes, could have been tried.

4.13.1 Runge-Kutta

The Runge-Kutta method numerically advances in time the solution a set

$$\frac{d\mathbf{y}}{dt} = \mathbf{F}(t, \mathbf{y}) \quad (175)$$

The vector \mathbf{y} has 6 components, and we assume the first 3 are those of δ , the last 3 those of \mathbf{u} . One can formally write

$$\frac{d\delta}{dt} = \mathbf{G} = \mathbf{u} \quad (176a)$$

$$\frac{d\mathbf{u}}{dt} = \mathbf{H} = \mathbf{H}(t, \delta) \quad (176b)$$

The function $\mathbf{H}(t, \delta)$ is the right-hand side of (13b), with q also a function of t and δ .

The essence of Runge-Kutta methods is to advance by small steps Δt , but design the steps cleverly so as to minimize error (in a similar sense, Simpson's rule is more clever than the trapezoidal rule). Perhaps the simplest member in the family of Runge-Kutta methods is the "Midpoint Method" which is important here because a slight modification of it, described below, plays a key role in the Bulirsch-Stoer method.

4.13.2 Modified Midpoint Method

Given a system of 1st order equations

$$\frac{d\mathbf{y}}{dx} = \mathbf{f}(\mathbf{y}) \quad (177)$$

one can extrapolate it from x to $x+2h$ by a simple Taylor term

$$\mathbf{y}(x+2h) = \mathbf{y}(x) + 2h \mathbf{f}(\mathbf{y}(x)) + O(h^2) \quad (178)$$

One gets a higher order approximation if instead of adding \mathbf{f} at x we add \mathbf{f} at the midpoint $x+h$ (functions without stated arguments are all at the initial point x):

$$\begin{aligned} f_i(\mathbf{y}(x+h)) &= f_i(\mathbf{y} + \Delta \mathbf{y}) = \\ &= f_i(\mathbf{y} + h \mathbf{f}(\mathbf{y})) = f_i(\mathbf{y}) + h \sum \frac{f_i}{dy_k} f_k \\ &= f_i(\mathbf{y} + h \mathbf{f}(\mathbf{y})) = f_i(\mathbf{y}) + h \sum \frac{f_i}{dy_k} \frac{dy_k}{dx} \\ &= f_i(\mathbf{y} + h \mathbf{f}(\mathbf{y})) = f_i(\mathbf{y}) + h \sum \frac{df_i}{dx} \\ &= f_i(\mathbf{y} + h \mathbf{f}(\mathbf{y})) = f_i(\mathbf{y}) + h \sum \frac{d^2 y_i}{dx^2} \end{aligned} \quad (179)$$

Substitute

$$\begin{aligned} y_i(x) + 2h f_i(\mathbf{y}(x+h)) &= y_i(x) + 2h f_i(\mathbf{y}) + 2h^2 \sum \frac{d^2 y_i}{dx^2} \\ &= y_i(x) + 2h \frac{dy_i}{dx} + \frac{1}{2} (2h)^2 \sum \frac{d^2 y_i}{dx^2} \end{aligned} \quad (180)$$

which is correct to order h^2 .

The *modified* midpoint method includes two small changes in this scheme, which actually make it less accurate, but (as will be seen) have their own reward: Start at x_0 with $\mathbf{y}(x_0)$ and let the step be h . Derive $\mathbf{y}(x+2h)$ to accuracy h^2 and $\mathbf{y}(x+h)$ only to order h (that is one modification):

$$\begin{aligned} \mathbf{y}_0 &= \mathbf{y}(x) \\ \mathbf{y}_1 &= \mathbf{y} + h\mathbf{f}(\mathbf{y}) && (\text{order } h \text{ only}) \\ \mathbf{y}_2 &= \mathbf{y} + h\mathbf{f}(\mathbf{y}_1) && (\text{order } h^2) \end{aligned} \quad (181a)$$

Then leapfrog

$$\begin{aligned} \mathbf{y}_3 &= \mathbf{y}_1 + h \mathbf{f}(\mathbf{y}_2) && (\text{uses } \mathbf{y}_1, \mathbf{y}_3 \text{ midpoint}) \\ \mathbf{y}_4 &= \mathbf{y}_2 + h \mathbf{f}(\mathbf{y}_3) && (\text{uses } \mathbf{y}_2, \mathbf{y}_4 \text{ midpoint}) \end{aligned}$$

etc. The last point again is modified. If $n+1$ is the last division (n segments of size h) then

$$\mathbf{y}(x + nh) = \frac{1}{2} (\mathbf{y}_n + \mathbf{y}_{n-1}) + \frac{1}{2} h \mathbf{f}(\mathbf{y}_n) \quad (181b)$$

4.13.3 "Classical" Runge-Kutta

Let $t \rightarrow t + \Delta t$. Then the "classical" RK prescription, accurate to order h^4 , calls for the following intermediate vectors $\mathbf{k}_i = (\mathbf{g}_i, \mathbf{h}_i)$, starting with

$$\mathbf{k}_1 = \Delta t \mathbf{F}(t, \mathbf{y}) = (\mathbf{g}_1, \mathbf{h}_1) = \Delta t (\mathbf{u}, \mathbf{H}(t, \delta)) \quad (182)$$

Initially, $\delta=0$, $u=0$, so $k_1 = (0, a\Delta t)$. In later steps, if the same osculating orbit is used, the initial values of (δ, u) are not in general zero, and k_1 is less simple.

The whole scheme (y means $y(t)$):

$$\begin{aligned} k_1 &= \Delta t F(t, y) \\ k_2 &= \Delta t F(t+\Delta t/2, y+k_1/2) \\ k_3 &= \Delta t F(t+\Delta t/2, y+k_2/2) \\ k_4 &= \Delta t F(t+\Delta t, y+k_3) \end{aligned}$$

and

$$y(t+\Delta t) = y(t) + \frac{1}{6} [k_1 + k_4 + 2(k_2 + k_3)] \quad (183)$$

For instance, starting from $(\delta, u) = (0, 0)$, we have (as derived below (16))

$$k_1 = (0, a(t)\Delta t) = (g_1, h_1) \quad (184a)$$

$$\begin{aligned} k_2 &= \Delta t F\left(t+\frac{\Delta t}{2}, y+\frac{k_1}{2}\right) = \Delta t F\left(t+\frac{\Delta t}{2}, \delta=0+\frac{g_1}{2}, u=0+\frac{h_1}{2}\right) \\ &= \Delta t F\left(t+\frac{\Delta t}{2}, \delta=0, u=\frac{a(t)}{2}\Delta t\right) \\ &= \left(\frac{a(t)}{2}\Delta t^2, a\left(t+\frac{\Delta t}{2}\right)\Delta t\right) = (g_2, h_2) \end{aligned} \quad (184b)$$

$$\begin{aligned} k_3 &= \Delta t F\left(t+\frac{\Delta t}{2}, y+\frac{k_2}{2}\right) = \Delta t F\left(t+\frac{\Delta t}{2}, \delta=0+\frac{g_2}{2}, u=0+\frac{h_2}{2}\right) \\ &= \Delta t F\left(t+\frac{\Delta t}{2}, \delta=\frac{a(t)}{4}\Delta t^2, u=\frac{1}{2}a\left(t+\frac{\Delta t}{2}\right)\Delta t\right) \\ &= \left(\frac{1}{2}a\left(t+\frac{\Delta t}{2}\right)\Delta t^2, H\left(t+\frac{\Delta t}{2}, \frac{a(t)}{4}\Delta t^2\right)\Delta t\right) = (g_3, h_3) \end{aligned} \quad (184c)$$

$$\begin{aligned} k_4 &= F(t+\Delta t, y+k_3) = \Delta t F(t+\Delta t, \delta=0+g_3, u=0+h_3) \\ &= \Delta t F\left(t+\Delta t, \delta=\frac{1}{2}a\left(t+\frac{\Delta t}{2}\right)\Delta t^2, u=H\left(t+\frac{\Delta t}{2}, \frac{a(t)}{4}\Delta t^2\right)\Delta t\right) \\ &= \left(H\left(t+\frac{\Delta t}{2}, \frac{a(t)}{4}\Delta t^2\right)\Delta t^2, H\left(t+\Delta t, \frac{1}{2}a\left(t+\frac{\Delta t}{2}\right)\Delta t^2\right)\Delta t\right) \end{aligned} \quad (184d)$$

Some of the terms are of order Δt^2 or smaller, but that is because this is just the first step after initial values $(0, 0)$. In any case, this sort of substitution is easy for a computer.

The iteration continues along the same osculating orbit, “rectifying” and replacing it with a new one whenever δ/r exceeds some limit ϵ , say 0.01. When that happens, the last point derived becomes the new starting point.

4.13.4 Runge-Kutta-Fehlberg

One big problem with the Runge-Kutta method is the estimation of the actual error. One can conduct the integration with step h and with step $h/2$ and compare, but that is rather wasteful, since the result we can trust is only accurate to order h .

A different approach was introduced by Fehlberg, who found a 6-step Runge-Kutta procedure whose terms in one combination integrated the differential equations to an accuracy of order h^5 and in another gave an accuracy of only order h^4 . Can these two solutions be meaningfully compared to provide an error

estimate of the less-accurate one? One may well be suspicious, since both use exactly the same terms, but in fact it was shown this is a perfectly acceptable way, and it is widely used today.

Numerical Recipes uses a scheme of this type by Cash and Karp, and also provides the codes. Their codes in addition use the error estimate to change the step-size h in the course of the calculation, increasing or reducing it to achieve a certain error range.

Unfortunately, the semi-major axis of the solution slowly changed, suggesting that the method was not accurate enough. Another Encke code, GRAVE, coded around 1985 by Roger Burrows at Marshall Space Flight Center, used Runge-Kutta integration, and it was applied by Mullins and Evans [1996] to plan orbits of the AXAF mission. Its semi-major axis also drifted, but its perigee variations were very close to those obtained with a non-drifting integration based on the method of Bulirsch and Stoer, as described below.

4.14 The method of Bulirsch and Stoer

The notes below are entirely based on chapters 3,4 and 16 of *Numerical Recipes*, and anyone interested in this approach is encouraged to consult that text. Bulirsch-Stoer method resembles Romberg integration and both rely on polynomial interpolation, described below.

4.14.1 Polynomial Interpolation (or extrapolation)

Given points $x_a(i), y_a(i)$, $i=1,2,\dots,n$, a unique polynomial $P(x)$ of degree $(n-1)$ exists which passes all the points (e.g. a straight line for $n=2$, parabola for $n=3$ etc.). Polynomial interpolation is the process by which $P(x)$ is found and its value at a particular x is derived.

A formula due to Laplace gives all the coefficients of $P(x)$, but its expressions are rather long. A easier way is to generate the coefficients is by **recursion**, using **Neville's algorithm**, which builds up $P(x)$ gradually through polynomials of lower degrees.

A great advantage of the algorithm is that it can work in either of two ways. We can build up the formula of $P(x)$ through polynomials of lower degree, **or** we can build up the value of $P(x)$ at a given value of x , given the values at x of the lower degree polynomials. In the first case we handle formulas, in the 2nd only numbers. Here are the details:

Given points $(x_1, y_1), (x_2, y_2) \dots (x_n, y_n)$ one can define as $P_{i(i+1)\dots(i+m)}$ the polynomial of degree m that fits the m consecutive points $[i, (i+1), \dots, (i+m)]$.

For instance: $P_1 = y_1 = \text{const.}$ is a polynomial of degree zero which fits (x_1, y_1) ; P_{23} is the linear polynomial fitting (x_2, y_2) and (x_3, y_3) . The final polynomial $P(x)$ being sought can also be written $P_{12\dots n}$.

Neville's recursion formula for $P_{i(i+1)\dots(i+m)}$ involves two polynomials of degree $(m-1)$, one of them missing (x_i, y_i) , the other missing (x_{i+m}, y_{i+m}) :

$$\begin{aligned}
 P_{i(i+1)\dots(i+m)}(x) &= \\
 &= \frac{1}{x_i - x_{i+m}} \left[(x - x_{i+m}) P_{i(i+1)\dots(i+m-1)}(x) + (x_i - x) P_{(i+1)\dots(i+m)}(x) \right] \\
 &= \frac{1}{x_i - x_{i+m}} \left[(x - x_{i+m}) a + (x_i - x) b \right] \tag{185}
 \end{aligned}$$

The left-hand polynomial, by its definition on (on the right), is of degree m , and is supposed to give $(y_i, y_{i+1} \dots y_m)$ at all the corresponding values of x .

Indeed, it does. For values of x other than those at the ends of the range, i.e. $x_{i+1}, \dots, x_{(i+m)-1}$, both a and b equal the appropriate y_k , the terms xa and $-xb$ cancel and we are left with just y_k . For $x=x_i$, $a=y_i$, and the term multiplying b is zero. For $x=x_{(i+m)}$ the same happens-- a does not matter, $b=y_{(i+m)}$. We can thus start the recursion with order-zero polynomials $P_i = y_i$ and build up.

A faster way is by defining "parent-daughter differences"

$$\begin{aligned} C_{m,i}(x) &= P_{i(i+1)\dots(i+m)}(x) - P_{i(i+1)\dots(i+m-1)}(x) \quad (\text{lower parent}) \\ D_{m,i}(x) &= P_{i(i+1)\dots(i+m)}(x) - P_{(i+1)\dots(i+m)}(x) \quad (\text{upper parent}) \end{aligned} \quad (186)$$

Then "*Numerical Recipes*" gives recursions

$$C_{m+1,i} = \frac{(x_i - x)(C_{m,i+1} - D_{m,i})}{x_i - x_{i+m+1}} \quad D_{m+1,i} = \frac{(x_{i+m+1} - x)(C_{m,i+1} - D_{m,i})}{x_i - x_{i+m+1}} \quad (187)$$

Using these, one only needs to trace *one* path from some chosen y_i to get to the peak of the pyramid and obtain $P(x)$.

Subroutine *polint* (xa, ya, n, z, y, dy) of *Numerical Recipes* generates the value $P(x)$ at some given x for the interpolating polynomial of the above array of point, using recursion. The error estimate is dy .

4.14.2 The Trapezoidal Rule

This is a rather simple scheme of numerically evaluating integrals, and is reviewed here only because it forms the foundation to Romberg integration, which in its turn has some similarities with the Bulirsh-Stoer method.

In this approximation, an integral s between given limits is estimated from a set of intermediate values, namely

$$s = \int_a^b f(x) dx \approx h \left[\frac{1}{2} f(a) + f(a+h) + f(a+2h) \dots + f(b-h) + \frac{1}{2} f(b) \right] \quad (188)$$

Subroutine *trapzd* ($func, a, b, s, n$) derives this approximation as output variable s , using 2^n equally spaced segments.

Note that by choosing to divide into 2^n segments, whenever one is forced to increase n , nothing is wasted, for all values of $f(x)$ already calculated can be reused. In what follows such values (e.g. those in (4) above) will be denoted f_0, f_1, \dots, f_n . The error here is of order h^2 .

4.14.3 The Euler-McLaurin summation formula

Numerical Recipes next cites a "deep fact" about the trapezoidal rule, known as the Euler-McLaurin summation formula. That formula states that not only is the difference between an integral and its trapezoidal approximation of order h^2 , but it can also be expanded in an asymptotic series *all* of whose terms are powers of h^2 , involving derivatives of odd degree of $f(x)$ at the end points:

$$\begin{aligned} \int_a^b f(x) dx - h \left[\frac{1}{2} f_0 + f_1 + \dots + \frac{1}{2} f_n \right] &= \frac{B_2 h^2}{2!} (f'_n - f'_1) + \frac{B_4 h^4}{6!} (f''_n - f''_1) + \dots \\ &\dots + \frac{B_{2k} h^{2k}}{(2K)!} (f^{(2k-1)}_n - f^{(2k-1)}_1) \end{aligned} \quad (189)$$

The coefficients are the Bernoulli numbers

$$B_0 = 1 \quad B_2 = 1/6 \quad B_4 = -1/30 \quad B_6 = 1/42 \quad B_8 = -1/30 \dots$$

generated by

$$\frac{t}{e^t - 1} = \sum B_n \frac{t^n}{n!} \quad (190)$$

From B_8 the terms grow larger again, without any limit, which is why the series **(189)** *does not* actually converge. But it is asymptotic, i.e. the error generated by truncating it is always less than twice the magnitude of the first neglected term.

Using the above series for (n) and (2n), one can eliminate the h^2 term and get an approximation to s which has only an h^4 error. The result is, in fact, Simpson's rule.

4.14.4 Romberg Integration

Romberg's method of evaluating integrals is an application of "Richardson's deferred approach to the limit." Suppose we derive a quantity s by a method involving a small parameter h ; Richardson's prescription is to carry out successive approximations s_1, s_2, \dots, s_n for a series of values h_1, h_2, \dots, h_n , fit them to an analytic function $s(h)$, then extrapolate $s(h)$ to the limit $s(0)$,

Romberg integration does this, using the trapezoidal rule **(4)**

$$s(h) = \int_a^b f(x) dx \approx h \left[\frac{1}{2} f(a) + f(a+h) + f(a+2h) \dots + f(b-h) + \frac{1}{2} f(b) \right]$$

Given approximations $s(h_k)$ for $h_k = (b-a)/2^k$, the method fits to $s(h)$ a polynomial of appropriate degree and extrapolates it to $h=0$.

There exists a twist, however: by the Euler-McLaurin formula we expect the polynomial to contain only **even** powers of y . So properly, the parameter on which s depends is not h but h^2 , or if we wish, $g = Ah^2$, with some convenient value of the constant A . We then derive as before values of s_1, s_2, \dots, s_n appropriate to g_1, g_2, \dots, g_n , fit the paired values to a polynomial $s(g)$, and as before, the optimal value is then obtained at $g=0$. The value of A is arbitrary, so we take $g_1 = 1, g_2 = 1/4 \dots g_{j+1} = 0.25 g_j$.

Subroutine *qromb* (*func, a, b, s*) on p. 134 carries this out. It derives the s_k for the values of g_k derived above (the book denotes them by h_i). Past a certain $K = KM$ (here $KM = 4$) it also calls subroutine *polint* to provide a polynomial approximation $P_k(g)$. It then derives the approximation $ss_k = P_k(0)$, and the error estimate $dss = ss_{k+1} - ss_k$. It stops when dss falls below some previously chosen criterion *EPS*.

4.14.5 The Modified Midpoint Method

The Bulirsch-Stoer integration applies the above approach to the solution of a system of coupled differential equations. As before, a sophisticated approximation to the solution is obtained, by extrapolating a series of simple approximations, depending on a small parameter h (or more accurately, on h^2) to its limit at $h = 0$.

The simple approximations in this case (analogous to the trapezoidal rule), is produced by the **modified midpoint method**, already described earlier. Given a set of equations

$$\frac{dy}{dx} = f(x, y) \quad (191)$$

this method advances the solution from x to $x+H$ (H need not be small) in n steps of $h = H/n$ each, by defining a sequence

$$\begin{aligned} \mathbf{z}_0 &= \mathbf{y}(x) \\ \mathbf{z}_1 &= \mathbf{z}_0 + h \mathbf{f}(x, \mathbf{z}_0) \\ \mathbf{z}_2 &= \mathbf{z}_0 + 2h \mathbf{f}(x+h, \mathbf{z}_1) \\ \mathbf{z}_3 &= \mathbf{z}_1 + 2h \mathbf{f}(x+2h, \mathbf{z}_2) \\ &\dots \dots \dots \\ \mathbf{z}_{k+1} &= \mathbf{z}_{k-1} + 2h \mathbf{f}(x+kh, \mathbf{z}_m) \end{aligned} \quad (192a)$$

and finally

$$\mathbf{y}(x+H) \approx \mathbf{y}_n = \frac{1}{2} [\mathbf{z}_n + \mathbf{z}_{n-1} + h \mathbf{f}(x+H, \mathbf{z}_n)] \quad (192b)$$

The midpoint method was described earlier, but here the first and last points are modified. A subroutine is provided to implement this method,

mmid (y, dydx, nvar, xs, htot, nstep, yout, derivs),

with *nvar* the number of variables, *xs* the starting value of x , (*xs+htot*) the final value (i.e. *htot*= H), *nstep* the number of substeps to be made and *yout* the output values: one may write \mathbf{y} in this position, in which case the output overwrites the input. Subroutine *derivs* provides the vector $\mathbf{f}(x, \mathbf{y})$.

The reason for the modification is that (as Gragg had shown) the error then (again) depends only on h^2 and can be approximated by a polynomial containing only even powers:

$$\mathbf{y}_n - \mathbf{y}(x+H) = \sum \alpha_i h^{2i} \quad (193)$$

As before, one can combine here approximations of order n and $2n$ and get one in which no h_2 term appears. In this case

$$\mathbf{y}(x+h) \approx \frac{1}{3} (4\mathbf{y}_{2n} - \mathbf{y}_n) \quad (194)$$

As with Romberg integration, this result is related to Simpson's rule.

4.14.6 The Bulirsch-Stoer Method

The Bulirsch-Stoer algorithm is the method of choice for advancing in time differential equations which involve *smooth* functions, while RK is a better choice for functions with corners or singularities. The authors also feel it is superior to predictor-corrector methods (described later). It is based on three ideas:

- (1) Richardson's deferred approach to the limit, i.e. extrapolation to $h=0$.
- (2) Rational approximation, i.e. representation as the ratio of two polynomials, which "breaks the shackles of power series." However, the
authors here have found that for smooth problems polynomials often work better; this is adopted here, although a subroutine *rzextr* is provided for the other way.
- (3) The use of expansions whose error depends only on h^2 , producing a faster approach to the solution.

The Bulirsch-Stoer method advances the solution of

$$\frac{d\mathbf{y}}{dx} = \mathbf{f}(x, \mathbf{y}) \quad (191)$$

by the modified midpoint method over a "macrostep H ", divided and redivided into "dozens to hundreds" of smaller "microsteps" h_1, h_2, \dots, h_n . This gives a series of approximations y_1, y_2, \dots for $y(x+H)$, which is extrapolated to $h=0$, or more accurately to $g = Ah^2 = 0$.

The number n_j of segments into which the range is divided in the j th step is **not** doubled each step, but grows more slowly. Bulirsch and Stoer proposed a modified doubling (n_j doubles every two steps)

$$n = 2, 4, 6, 8, 12, 16, 24, 32 \dots \quad n_j = 2n_{j-2} \quad (195a)$$

which alternates two doubling sequences, 2,4,8,16,32.. and 6,12,24,48,... Deuffhard (1983, 1985) suggested instead

$$n = 2, 4, 6, 8, 10, 12, 14, 16 \dots \quad n_j = 2j \quad (195b)$$

which is usually more efficient. The big question is choosing the right H : too small is an inefficient use of a powerful method, too big and the method does not converge. The rule adopted here is to proceed 8 steps, to $n=16$, and if the error does not seem to shrink, go to a smaller H ,

Numerical Recipes goes into some details of how this choice of H works, and also provides a subroutine

bsstep (*y,dydx,nv,x,htry,eps,yscal,hdid,hnext,derivs*)

which calls ***mmid*** (above) and either ***pzextr*** for polynomial extrapolation, or ***rzextr*** for rational function extrapolation. It is configured so that it can replace in subroutine ***odeint*** a subroutine ***rkqs*** which advances step by step using the Runge-Kutta method.

As before, nv is the number of variables, $htry$ is the initial step size, ***yscal*** is vector against which $\Delta y = yerr$ is scaled (in the DO 16 loop), $hdid$ is the step actually used and $hnext$ the estimated next stepsize, which should become $htry$ of the Bulirsch-Stoer code for the next step.

4.16.7 Multistep (MS), Multivalue (MV) and Predictor-Corrector (PC)

MS and MV methods are two equivalent ways of implementing a specific technique for solving ODEs. The "predictor-corrector" (PC) method is the most popular one of this type, so often all such methods are referred to as "predictor-corrector". They are best for high-precision work with very smooth equations, but "bookkeeping details are the bane."

In RK or BS, a single step $x \rightarrow x+h$ or $x \rightarrow x+H$ is subdivided and advanced. In **multistep** methods the combined record of several past points is involved in each advance. Suppose the equations to be solved are

$$\frac{dy}{dx} = f(x,y) \quad (196)$$

The solution has reached y_n and must now be advanced to y_{n+1} . Formally

$$y_{n+1} = y_n + \int_{y_n}^{y_{n+1}} f(x,y) dx \quad (197)$$

and one might approximate it by a Taylor expansion

$$y_{n+1} = y_n + h f(y_n, x) \quad (198)$$

A better approximation would be

$$\mathbf{y}_{n+1} = \mathbf{y}_n + \frac{1}{2} h [\mathbf{f}(\mathbf{y}_{n+1}, \mathbf{x}) + \mathbf{f}(\mathbf{y}_n, \mathbf{x})] \quad (199)$$

where \mathbf{y}_n on the right-hand side is taken from the approximation (198).

That however is very crude. The general PC method therefore replaces (199) by

$$\mathbf{y}_{n+1} = \mathbf{y}_n + h[\beta_0 \mathbf{f}_{n+1} + \beta_1 \mathbf{f}_n + \beta_2 \mathbf{f}_{n-1} + \beta_3 \mathbf{f}_{n-2} + \dots] \quad (200)$$

To predict \mathbf{y}_{n+1} on the right of (18) we extrapolate it from earlier values of \mathbf{y} using some polynomial scheme. A popular scheme is the Adams-Moulton-Bashford method; Adams and Moulton were astronomers, suggesting this method was widely applied to the integration of orbits, and [Danby \[1992\]](#) describes such uses in section 10.7. The 3rd order equations have a predictor

$$\mathbf{y}_{n+1} = \mathbf{y}_n + \frac{h}{12} [23 \mathbf{f}_n - 16 \mathbf{f}_{n-1} + 5 \mathbf{f}_{n-2}] + O(h^4) \quad (201a)$$

and the corrector

$$\mathbf{y}_{n+1} = \mathbf{y}_n + \frac{h}{12} [5 \mathbf{f}_{n+1} + 8 \mathbf{f}_n - \mathbf{f}_{n-1}] \quad (201b)$$

Note that in each case the coefficients add up to 12, just as in (199) they add up to 2, since these are all improvements on the crude (198). The authors recommend against repeated iteration, which only gives marginal improvement. Higher orders PC schemes also exist.

4.15 Derivation of the Perturbed Orbit

4.15.1 The ENCKE code

A Fortran code ENCKE was produced to integrate the equations of Encke's method. The code contained three sections: input, integration and output.

The input section read the starting conditions, either from a data file or from the keyboard. These included starting date, the length of the run and starting conditions, presented in one of three ways: (1) entry time into parking orbit, exit condition from that orbit and velocity at exit, or (2) initial time and $(\mathbf{r}_0, \mathbf{v}_0)$, or (3) initial time and osculating elements. This section also included various preparatory steps, e.g. the preparation of an initial array of positions of the Moon and the Sun.

The basic output was a file containing all sets of osculating elements derived for the motion, each with the elapsed time at which it became effective. That information allowed the reconstruction of (\mathbf{r}, \mathbf{v}) for any time t covered by the calculation, as soon as the set of elements appropriate for that time was located, which only required a binary search. For instance, given two such sequences for two satellites initially on the same orbit but passing perigee one hour apart, these data make it possible to track the changes in their separation throughout the period covered by them.

The main problem with this output was its size, since typically osculating elements were switched once a day. A second output, more manageable and short enough to be scanned by eye, was therefore provided on the standard output file, which also recorded various initial parameters. That output listed time, perigee distance, semi-major axis, eccentricity, inclinations to the equator and ecliptic, the angles χ_1 and χ_2 , etc. The entries of that list was separated by uneven intervals, always longer than some specified length t_1 , e.g. 30 or 60 days. After a set of output parameters was listed (and this was always done for the initial time $t=0$), the code waited a time t_1 , after which the wait continued until the next set of osculating elements was produced, and that set gave the output next on the list.

The integration section was the longest part of the code and was handled entirely by subroutines. The link between them and ENCKE was through ODEINT (Ordinary Differential Equations INTegration), adapted from *Numerical Recipes*. It was written in a way suitable for either the Runge-Kutta subroutine RKQS or

the Bulirsch-Stoer subroutine BSSTEP, both of which were supplied by the book, as were the subroutines required by them. Some details of these algorithms and codes are given in **Appendix C**.

Either method works with the 6 equations (), whose time derivatives depend on the preceding values of (δ, \mathbf{u}) , the osculating orbit and the time t . The first 3 equations

$$\frac{d\delta}{dt} = \mathbf{u} \quad (176a)$$

are trivial, since the preceding \mathbf{u} is known explicitly. However, the other three

$$\frac{d\mathbf{u}}{dt} = \mathbf{a} + \text{etc.} \quad (176b)$$

require \mathbf{r}_{osc} , the position at time t in the osculating orbit, as well as the perturbing acceleration \mathbf{a} , for which the positions of the Sun and Moon must be provided.

All that is handled by subroutine DERIVS, which is the core of the calculation. It also handles the derivation of new osculating elements (“rectification” of the variables) whenever it is needed. Both with Runge-Kutta and Bulirsch-Stoer, DERIVS is called several times in each step (more in Bulirsch-Stoer, where “macrosteps” are larger), and those intermediate times are obviously not appropriate for testing δ and possibly introducing new elements. The subroutine is however also called once at the beginning of each step by ODEINT itself, and that is where the test is performed. If δ is large enough to make the osculating orbit further away from the true one than what has been allowed, the current values of (δ, \mathbf{u}) are added to the osculating $(\mathbf{r}_{\text{osc}}, \mathbf{v}_{\text{osc}})$ to give the perturbed (\mathbf{r}, \mathbf{v}) , new elements are derived from the new perturbed values and (δ, \mathbf{u}) are reset to zero.

Whenever the orbit is thus “rectified” the new elements are passed to ODEINT, which stores them in arrays later passed to the output. All sorts of small modifications exist here, e.g. rectification was postponed when it was demanded close to perigee (see further below), and it was enforced automatically if it failed to occur within a preset time interval after the preceding rectification.

In any numerical calculation, an independent check on the accuracy of the result is always valuable. In celestial mechanics, in the presence of purely periodic perturbations, the semi-major axis may fluctuate but its average value should stay fixed. With the Runge-Kutta method, it slowly drifted; the drift rate could be reduced by forcing smaller steps, but it was always present. After that the Bulirsch-Stoer method was substituted, and ultimately it passed the test.

At first, however, the codes of *Numerical Recipes* ran into a problem. For both integration schemes, they adjusted their step size to meet certain error bounds, using their internal error estimates. Whenever a new set of osculating elements was introduced, the process started anew, beginning with an extremely small step size. However, the procedure then did not converge in an orderly way to the appropriate macrostep (typically 10 hours), possibly because initially the osculating orbit and the real one were extremely close. “Priming the pump” with steps of 1-10 seconds eliminated the problem.

4.15.2 The periodic variation of the semi-major axis

When the program finally ran, the semi-major axis a seemed stable, but a strange feature was noted. Its value seemed to fluctuate appreciably, giving the plot of a against time an appreciable thickness, on which short “hairs” were randomly superimposed. At the same time it was noted that the initial osculating value of a , at $t=0$, was abnormally high: it seemed as if a had slumped during the first few minutes of the orbit and afterwards varied only randomly, by smaller amounts.

The feature was traced to the oblateness of the Earth and when oblateness terms in \mathbf{a} were switched off, it disappeared. Because motion in the field of the oblate Earth departs from a Kepler ellipse, its osculating semi-major axis varies periodically around the orbit. Like the attraction of the equatorial bulge, the effect

peaked near perigee and quickly subsided at greater distances. The peak in a observed at $t=0$ was thus a periodic affair, associated with the perigee pass (the orbit was always started at perigee) and not with the beginning of the calculation. Similar peaks were observed at other perigee passes, but since the main effect was only noted 20 minutes from perigee, they were rarely encountered by chance at later passes and the code had to be modified (by forced rectifications near perigee) to make them visible. For this reason, too, the random fluctuation of a dropped when rectifications were postponed when ever they were called for within 2 hours of a perigee pass (which covered about 8% of the orbit).

The periodical variation of a due to the Earth's bulge also produced a problem when a code ENCKE12 was developed from ENCKE, tracking for one year 12 satellites in the same initial orbit; the 1-year time-span was chosen. because the outputs were then to be analyzed for magnetospheric coverage, shadows and the occurrence of specific constellations, the way Keplerian orbits were handled at an earlier stage.

It is worth noting that when the perturbation due to the Earth's oblateness was removed, the semi-major axis stayed nearly constant even when Runge-Kutta integration was used. Thus this effect may also be implicated in the problems attending the use of the Runge-Kutta method.

Because the initial orbit was the same, it was expected that all satellites could be started with the same osculating elements (a, e, i, ω, Ω), but with the mean anomaly l separated by fixed amounts--e.g. separations of $2\pi/T$ radians, with T the orbital period in hours, would cause the satellites to pass perigee one hour apart. When this was put into practice, however, it turned out that small differences existed then in the orbital periods, causing the relative positions of satellites to drift, in a few cases even causing satellites to overtake each other.

This too was caused by the periodic variation of a . In strict Keplerian motion, T is a function of a (Kepler's third law) and should therefore be the same for all satellites. Due to the equatorial bulge, however, osculating a varied systematically around the orbit. Orbits with the same a at perigee and the same perigee distance then still have the same T , but the actual orbits had different values of a at perigee, because their initial values of a were specified to be equal at some other points in their orbits, and these points differed for each satellite.

4.15.3 ENCKE12A and ORB7

To overcome this problem, a variant code ENCKE12A was produced, specifying as initial condition not the orbital elements of each satellite, but only those of the "bus" releasing the satellites at consecutive perigee passes, as well as the value of Δv imparted at release. One great advantage of this approach was that the effects of a "centrifugal slingshot" release were readily incorporated, by assuming the satellites were released two at a time, with velocity increments $\pm \Delta v$. For simplicity, the orbit of the "bus" was assumed to be purely Keplerian: because all releases were at perigee, where the "bus" orbit originally began, the injection velocities were unaffected. However, the small difference between the orbital period of the Keplerian motion and the one with the bulge present were not taken into account. The difference made by this is small, because within 5 periods of the "bus" all releases are complete.

In either 12-satellite code ODEINT is called separately to integrate the orbit of each satellite, up to some final time t_f . When the run is complete, ODEINT always provides the final values of (δ, \mathbf{u}) , and adding these to the final osculating $(\mathbf{r}_{osc}, \mathbf{v}_{osc})$ produces the final (\mathbf{r}, \mathbf{v}) . These can then be saved in a separate output file (together with the time and other details) to serve as starting conditions for the call of ENCKE12 for the next year, either explicitly as written above or implicitly through the starting values of the osculating elements ($a, e, l_0, i, \omega, \Omega$), which convey the same information.

ENCKE12A was intended to be no more than an initializing code, covering a short period (e.g. 2 weeks), after which all satellites are in orbit, with their simultaneous positions at the end of the period specified. After that ENCKE12 was called for one year at a time, and its output files served as input to ORB7, a code resembling ORB5 or ORB6, providing statistics of annual coverage of various magnetospheric regions and of shadows and constellations. ORB7 differed from earlier codes in that for each hour covered, the actual

position of each satellite must be calculated, not merely permuted among a small number of pre-calculated locations. In ORB7 that is accomplished rather quickly, using the tabulated sets of osculating element for each satellite. In a given hour, those values are usually either the same as the one used the preceding hour, or those of the next set in the tabulation, so that a long search for the appropriate set is usually not needed.

4.16 The Perturbed Orbit (tentative)

(This section will describe results learned from the application of the codes. Some things have not yet been tested, and even where results exist, I have run too few orbits and should get a good sample to confirm the conclusions)

4.16.1 Perigee height

The perigee height of the perturbed orbit changes on two characteristic time scales--a semi-annual oscillation of typical peak-to-peak amplitude of 500 km and a long-term variation with typical period of 5-9 years, both of these reflecting corresponding oscillations in the orbital eccentricity.

Such behavior was found by Mullins and Evans [1996] who used the Encke code GRAVE for a 50-year span of a sample AXAF orbit (Figure 3, loc.cit.). They found a growing oscillation in eccentricity and perigee altitude, apparently ultimately causing the perigee to enter the atmosphere after some decades and the satellite to decay. The perigee variation was duplicated by ENCKE. It did not however yield the drift of a shown in the published article, which was probably a spurious effect due to the use of the Runge-Kutta method. Such long-term behavior **(is typical)(is not typical)**.

Presumably it is desirable to inject the "Profile" bus at the lowest perigee possible, since raising perigee requires either more fuel or a lighter payload. A good strategy seems to be to choose some initial (ω, Ω) based on expected (initial) magnetospheric coverage, calculate the orbit for launch at some appropriate time and then shift the launch date to fit the minimum time of the semi-annual oscillation in perigee height. Such a shift will make perigee height rise after launch, whereas a launch near the top of the cycle would be followed by a drop, probably reducing the orbital lifetime.

(the following is just a guess and must be demonstrated!)

On a longer time scale, it helps to locate the minima of the long-term oscillations and launch then. Because of the synergy between "Profile" and almost any other magnetospheric mission, it is highly desirable to have the mission last as long as possible. In practice, a lifetime of the order of 10 years is probably a reasonable goal: in comparison ISEE 1/2, launched with perigee (**give value**) km, lasted about 8.5 years (**check**).

Then: Results of tests.

- Variability of spacing between satellites.

- Variations of i_e, χ_1, χ_2 etc.

- Some sample missions, with coverage figures.